Synchronization effects on rest frame energy and momentum densities in the proton

Adam Freese[1,2,*] and Gerald A. Miller[2,†]

[1]*Theory Center, Jefferson Lab, Newport News, Virginia 23606, USA*
[2]*Department of Physics, University of Washington, Seattle, WA 98195, USA*

We obtain two-dimensional relativistic densities and currents of energy and momentum in a proton at rest. These densities are obtained at surfaces of fixed light front time, which physically corresponds to using an alternative synchronization convention. Mathematically, this is done using tilted light front coordinates, which consist of light front time and ordinary spatial coordinates. In this coordinate system, all sixteen components of the energy-momentum tensor (when written in the mixed representation) obtain clear physical interpretations, and the nine Galilean components reproduce results from standard light front coordinates (several of which we report for the first time). We find several optical synchronization effects that are absent in instant form densities, indicating motion within the target. Spin-zero and spin-half targets both exhibit an internal longitudinal energy flux related to the $D(t)$ form factor, and transversely-polarized spin-half targets exhibit an energy dipole moment—which evaluates to $-1/4$ for all targets if the Belinfante EMT is used, but which is target dependent and vanishes for pointlike fermions if the asymmetric EMT is instead used.

I. INTRODUCTION

Significant attention has been placed on the energy momentum tensor (EMT) and the associated gravitational form factors [1] over the past few years. Major questions in the field of hadron physics, such as the proton mass puzzle [2–8] and proton spin puzzle [9–13] are directly related to the EMT. Additionally, there has been much discussion over how (and whether) the EMT encodes distributions of static forces within hadrons [8, 14–18]. This attention is especially pertinent with the anticipated construction of the Electron Ion Collider [19–21], since the measurement of generalized parton distributions [22–24] is the most promising means of empirically accessing the gravitational form factors.

Currently the literature is filled with a variety of perspectives on how to obtain spatial distributions of local currents in composite systems, including those encoded by the EMT (see for instance Refs. [15, 16, 25–35]). The light front formalism stands out among these as providing relativistically exact 2D densities [36, 37] that are obtained from elementary field-theoretic definitions [17, 26] in a wave-packet-independent way [31]. Misgivings have been expressed about the light front densities with the understanding that they constitute a description of the system moving at infinite momentum [38]. However, in a recent work [33], we showed that light front densities constitute *rest frame densities* within hadrons at a fixed light front time by utilizing a coordinate system called tilted light front coordinates (or tilted coordinates):

$$\tau = x^0 \equiv t_{\mathrm{IF}} + z_{\mathrm{IF}} \tag{1a}$$
$$x = x^1 \equiv x_{\mathrm{IF}} \tag{1b}$$
$$y = x^2 \equiv y_{\mathrm{IF}} \tag{1c}$$
$$z = x^3 \equiv z_{\mathrm{IF}}\,, \tag{1d}$$

first proposed by Blunden, Burkardt and Miller [39]. By using light front time τ but ordinary Cartesian spatial coordinates (x, y, z), the Galilean subgroup of the Poincaré group can be exploited while utilizing everyday intuition about space, including that a target is at rest when $(v_x, v_y, v_z) = (0, 0, 0)$.

Operationally, the use of tilted coordinates corresponds to synchronizing spatially distant clocks under the assumption that the speed of light is infinite in the $-z$ direction, and consequently the light front densities constitute a literal picture of what an observer looking in the $+z$ direction sees when their local time is τ. In our prior work [33] we refer to this synchronization rule as *light front synchronization*. Light front synchronization stands in contrast to the standard Einstein synchronization convention [40], under which spatially distant clocks are synchronized by assuming that the one-way speed of light is isotropic and equal to c in all directions. Using Einstein synchronization results in the standard Minkowski (or instant form) coordinate system, in which the observer is understood to see a past state of the system they are observing. (See Refs. [41–45] for detailed discussions of synchronization conventions.)

Previously, we obtained the rest frame electromagnetic currents of the proton and neutron in tilted light front coordinates [33]. The purpose of the present work is to obtain the energy and momentum currents encoded by the EMT within the same formalism.

* afreese@jlab.org
† miller@uw.edu

	Component	Breit frame	Standard light front	Tilted coordinates
Energy density	$T^0{}_0(\boldsymbol{x})$	Eq. (17a) of [15]	—	Eq. (2)
Momentum density	$-T^0{}_i(\boldsymbol{x})$	Eq. (17c) of [15]	Eqs. (11) & (20) of Ref. [47] [long.] same as Eq. (65b) [trans.]	Eq. (65)
Energy flux density	$T^i{}_0(\boldsymbol{x})$	same as Eq. (17c) of [15]	same as Eq. (69) [trans. only]	Eq. (69)
Stress tensor	$-T^i{}_j(\boldsymbol{x})$	Eq. (17b) of [15]	Eq. (21) of [47] [trans. only]	Eq. (70)

TABLE I. Explicit results for EMT densities of spin-half targets in the Breit frame formalism, the standard light frame formalism, and in tilted coordinates can be found in the references and equations provided in this table. The references have been chosen for easy consultation and for providing formulas for arbitrary polarization, rather than for original discovery. In several cases, standard light front results do not exist, or only exist for transverse components. Reference [16] provides a light front P^- density in its Eq. (107), but is excluded from the table because $P^- \neq E$ and because the result is only for unpolarized targets. In several other cases, standard light front densities are obtainable, but we could not find results for them in the literature, so we have pointed to equivalent formulas in the present work.

A variety of EMT densities already exist in the literature in different formalisms, but the tilted coordinate framework offers a number of advantages that make the presentation of new EMT densities worthwhile. Much like the standard light front densities, the densities obtained in tilted coordinates are relativistically exact, while the more commonly-used Breit frame densities are leading-order contributions that dominate for spatially diffuse wave packets [29, 31], and are as such subject to relativistic corrections [15]. Moreover, when localizing wave packets in instant form coordinates, the resulting densities differ from the Breit frame densities [32, 35, 46], since the dominating term in an infinite series differs for localized wave packets [29]. The standard light front and tilted light front densities, by contrast, are fully independent of the target's wave packet [31, 33].

There are also several advantages to using tilted light front coordinates over standard light front coordinates when obtaining densities. One of these is the ability to clearly show that the results are rest frame densities. Additionally, for local currents such as the electromagnetic current $j^\mu(x)$ and the energy-momentum tensor $T^{\mu\nu}(x)$, every component of the current obtains a clear physical interpretation in tilted coordinates. By contrast, the components $j^-(x)$, $T^{i-}(x)$ and $T^{--}(x)$ do not have clear interpretations in standard light front coordinates, and accordingly are typically ignored. In this work, we will present results for all sixteen components of the proton's EMT density.

One last benefit of tilted coordinates over standard light front coordinates is that the tilted energy E is exactly equal to the standard instant form energy, and that the tilted energy density

$$\mathcal{E}(\boldsymbol{b}_\perp, \hat{\boldsymbol{s}}) = m \int \frac{\mathrm{d}^2\boldsymbol{\Delta}_\perp}{(2\pi)^2} \Bigg(A(-\boldsymbol{\Delta}_\perp^2) + \frac{\boldsymbol{\Delta}_\perp^2}{4m^2} D(-\boldsymbol{\Delta}_\perp^2) + \frac{(\hat{\boldsymbol{s}} \times \mathrm{i}\boldsymbol{\Delta}_\perp)\cdot \hat{e}_z}{2m} \left\{ B(-\boldsymbol{\Delta}_\perp^2) - J(-\boldsymbol{\Delta}_\perp^2) - \frac{\boldsymbol{\Delta}_\perp^2}{4m^2} D(-\boldsymbol{\Delta}_\perp^2) \right\} \Bigg) \mathrm{e}^{-\mathrm{i}\boldsymbol{\Delta}_\perp \cdot \boldsymbol{b}_\perp} \tag{2}$$

is thus an exact 2D relativistic distribution of the usual energy E, rather than of P^-. The tilted energy density is thus more pertinent to debates about the proton mass decomposition, which typically frame the mass decomposition as an energy decomposition [2–4, 6–8]. (Eq. (2) will be proved below in Sec. V after the necessary formalism has been developed. Table I can be consulted to quickly find explicit results to the EMT densities, as well as their analogues in standard light front coordinates and the Breit frame formalism.)

The EMT densities in tilted coordinates also feature a variety of optical effects arising from light front synchronization. These features are shared in common with standard light front coordinates, but their status as optical synchronization effects rather than kinematic artifacts due to boosting the target is made clearer in tilted coordinates. A previously-explored example of an optical synchronization effect is the $\sin\phi$ modulations in the charge densities of transversely-polarized targets [33]. In general, optical synchronization effects occur when there is internal motion in the target, and accordingly are a promising indicator of partonic motion. In fact, we will show that a longitudinal energy flux density that depends solely on the $D(t)$ form factor arises as an optical synchronization effect, suggesting that $D(t)$ actually encodes internal motion. Notably, the form factor $D(t)$ is widely believed to be related to internal pressures [8, 14–17]. Its appearance in an optical synchronization effect therefore suggests that the internal pressure may be due to partonic motion in a similar manner to how hydrostatic pressure in gases and fluids arises from molecular motion. This raises doubts as to whether these internal pressures can provide any information about long-range forces or confinement.

Tilted coordinates are a counter-intuitive coordinate system with peculiar properties, and this work is not intended as an introduction to them. We have compiled a collection of helpful basic properties and identities in Appendix A for easy access, but a full exposition of the coordinate system is given in Ref. [33]. The remainder of this work uses tilted coordinates, and contains occasional reminders of their idiosyncratic properties.

This work is organized as follows. In Sec. II, we explain how components of the energy-momentum tensor are interpreted as furnishing densities and flux densities of energy and momentum, and provide a dictionary for converting components of the EMT into energy and momentum currents. In Sec. III, we explore how expectation values of the EMT for physical states can be decomposed into an internal rest-frame distributions and state-dependent smearing functions, the latter of which absorbs dependencies on the target's overall motion. Next, in Sec. IV, we obtain the rest frame energy and momentum currents for a spin-zero target as a warm-up exercise. Sec. V then provides expressions for the rest frame EMT densities of a spin-half target as well as numerical examples for a proton. Finally, we conclude in Sec. VI.

Throughout this work—and in contrast to our previous work on the subject [33]—we do not include any special markings (such as a tilde) to indicate that tilted coordinates are being used. Unless explicitly indicated otherwise (such as by a subscript or superscript IF for "instant form"), all non-invariant quantities should be assumed to signify a quantity in tilted coordinates.

II. ENERGY AND MOMENTUM CURRENTS IN TILTED COORDINATES

The energy-momentum tensor (EMT) is a local operator characterizing the distribution and flow of energy and momentum of a system. In quantum chromodynamics (QCD), the operator is formally given by [11, 48]:

$$\hat{T}^{\mu\nu}_{\text{QCD}} = \sum_q \frac{i}{4}\bar{q}\gamma^{\{\mu}\overleftrightarrow{D}^{\nu\}}q + F^{\mu\rho}_a F^{a\,\nu}_{\rho} - A^{\{\mu}_a(\partial^{\nu\}}B_a - i(D^{\{\mu}c)(\partial^{\nu\}}\bar{c}) - g^{\mu\nu}\mathscr{L}_{\text{QCD}}\,, \tag{3}$$

where $\mathscr{L}_{\text{QCD}}$ is the QCD Lagrangian:

$$\mathscr{L}_{\text{QCD}} = \sum_q \bar{q}\left(\frac{i}{2}\overleftrightarrow{\partial\!\!\!/} + g A\!\!\!/_a T^a - m_q\right)q - \frac{1}{4}F^a_{\mu\nu}F^{\mu\nu}_a - (\partial_\mu B_a)A^\mu_a + \frac{\alpha_0}{2}B^2_a - i(\partial_\mu\bar{c}^a)(D^\mu_{ab}c^b)\,. \tag{4}$$

Here A^μ_a is the gluon four-potential, B_a are Lagrange multiplier fields and c_a and $\bar{c}_a$ are the Faddeev-Popov ghosts. The Lagrange multiplier and ghost fields are unphysical and annihilate physical states, but are necessary to quantize and renormalize the theory [48]. The different representations of the gauge-covariant derivative are:

$$\overrightarrow{D}_\mu q = \overrightarrow{\partial}_\mu q - igA^a_\mu T_a q \tag{5a}$$

$$\bar{q}\overleftarrow{D}_\mu = \bar{q}\overleftarrow{\partial}_\mu + ig\bar{q}A^a_\mu T_a \tag{5b}$$

$$D^{ab}_\mu c^b = \Big(\delta_{ab}\partial_\mu + gf_{acb}A^c_\mu\Big)c^b\,, \tag{5c}$$

and the gluon field strength tensor is:

$$F^a_{\mu\nu} = \partial_\mu A^a_\nu - \partial_\nu A^a_\mu + gf_{abc}A^b_\mu A^c_\nu\,. \tag{6}$$

Here, T_a are the generators of the color $\mathfrak{su}(3,\mathbb{C})$ algebra and f_{abc} are the totally antisymmetric structure constants defined by:

$$[T_a, T_b] = if_{abc}T_c\,. \tag{7}$$

The EMT can be derived through several methods. Noether's first theorem and invariance of the QCD action under global spacetime translations infamously results in an EMT that is not gauge invariant [11, 24, 48], but this is rectified through the Belinfante improvement procedure [49], which adds a trivially conserved quantity to the EMT in order to restore gauge invariance. The trivially conserved quantity is usually chosen to reproduce Eq. (3). However, Leader and Lorcé [11] show that an alternative EMT can be obtained, with an additional antisymmetric piece:

$$\hat{T}^{\mu\nu}_{\text{asym}}(x) = \hat{T}^{\mu\nu}_{\text{QCD}}(x) + \sum_q\left\{\frac{1}{2}\bar{q}(x)\gamma^{[\mu}\,\mathrm{i}\overleftrightarrow{D}^{\nu]}q(x)\right\} \equiv \hat{T}^{\mu\nu}_{\text{QCD}}(x) + \hat{T}^{\mu\nu}_{\text{A}}(x)\,. \tag{8}$$

The antisymmetric piece is interpreted as describing intrinsic fermion spin; see Ref. [11] for further details.

The EMT can alternatively be derived using Noether's second theorem while assuming invariance of the QCD action under local spacetime translations[50]. If fermion fields transform according to their Lie derivative under these local translations, the resulting EMT is exactly that in Eq. (3). The EMT in Eq. (3) can also be obtained by taking the functional derivative of the QCD action with respect to the metric tensor [24] or with respect to the vierbein [48]. These methods avoid the need for an improvement procedure to ensure gauge invariance, and lack an ambiguity about the resulting EMT.

Regardless of whether the antisymmetric piece $\hat{T}^{\mu\nu}_{\text{A}}(x)$ is included in the EMT, integrals of the EMT over equal-time surfaces reproduce the generators of spacetime translations, as a consequence of being the conserved Noether current associated with spacetime translation symmetry. If V is a fixed-time hypersurface and n_μ is a unit forward-directed normal to this surface:

$$\hat{P}^\nu(\tau) = \int_V \mathrm{d}^3\boldsymbol{x}\, n_\mu \hat{T}^{\mu\nu}(x,\tau)\,, \tag{9}$$

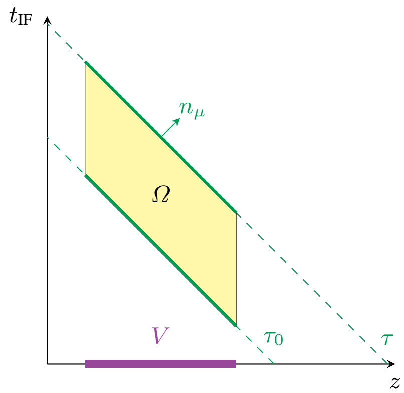

FIG. 1. A finite spacetime region Ω bounded by two hypersurfaces of equal light front time τ_0 and τ, drawn in terms of instant form coordinates. Each slice of fixed light front time contains the same spatial region V. The future-directed normal n_μ to the equal-light-front-time hypersurfaces is also indicated in this diagram.

where τ is the time variable under consideration. If instant form time (the time resulting from Einstein synchronization) is used to define equal-time surfaces, then n_μ is a timelike vector pointing in the forward-t_{IF} direction. If light front time $t_{\mathrm{IF}} + z$ is instead used to define equal-time surfaces, n_μ is a lightlike vector pointing along the light cone. The latter scenario is depicted with a finite hypersurface in Fig. 1. If V is extended to all of space, then $\hat{P}^\nu$ is conserved, and thus time-independent, by virtue of Noether's theorems.

The four-vector operator $\hat{P}_\nu$ plays the role of a spacetime translation generator, specifically in its covariant form (with a lower index):

$$\mathrm{i}[\hat{P}_\nu, \hat{O}(x)] = \partial_\nu \hat{O}(x) \,. \tag{10}$$

The contravariant (upper-index) components of the four-momenta are related to the covariant components through $\hat{P}^\nu = g^{\nu\rho}\hat{P}_\rho$. In instant form coordinates, this gives a trivial relationship for components of the vector momentum:

$$\hat{\boldsymbol{P}}_{\mathrm{IF}} = (\hat{P}^1_{\mathrm{IF}}, \hat{P}^2_{\mathrm{IF}}, \hat{P}^3_{\mathrm{IF}}) = (-\hat{P}^{(\mathrm{IF})}_1, -\hat{P}^{(\mathrm{IF})}_2, -\hat{P}^{(\mathrm{IF})}_3) \,, \tag{11}$$

but in tilted coordinates the relationship is more complicated—see Eq. (A2) for the metric tensor in tilted coordinates and Eq. (A3) for the covariant-contravariant relations. In order to play their proper role as space translation generators, components of vector momentum are identified through *covariant* components of the four-momentum: $\hat{\boldsymbol{P}} = (-\hat{P}_1, -\hat{P}_2, -\hat{P}_3)$. Likewise, the Hamiltonian (as the time translation generator) is given by $\hat{P}_0$. Accordingly, the energy and momentum densities are associated with the mixed upper-lower form of the EMT, $\hat{T}^\mu{}_\nu(x)$, which can be interpreted as a $\hat{P}_\nu$ current. As such, $\hat{T}^\mu{}_0(x)$ gives an energy-four current—a combination of an energy density and energy flux density—while $-\hat{T}^\mu{}_i(x)$ encodes three vector momentum currents.

As is standard in continuum mechanics [51–56], flux densities of momentum can be interpreted as stresses. We review the rationale behind this. By virtue of Noether's theorems, the EMT obeys a continuity equation:

$$\partial_\mu T^\mu{}_\nu(x) = 0 \tag{12}$$

which is the differential form of energy-momentum conservation. If we integrate this differential form over the spacetime region Ω depicted in Fig. 1 and use the divergence theorem, we obtain the integral form of the conservation law:

$$\frac{\mathrm{d}}{\mathrm{d}\tau}\left[T^0{}_\nu(\boldsymbol{x},\tau)\right] = -\oint_{\partial V} \mathrm{d}A_i \, T^i{}_\nu(\boldsymbol{x},\tau) \,, \tag{13}$$

where ∂V is the boundary of the spatial region V and $\mathrm{d}\boldsymbol{A}$ is an area element with outward-pointing normal. This equation describes the amount of P_ν in a spatial region V changing due to the flux of P_ν through the boundary of this region. For this reason, $T^0{}_\nu(\boldsymbol{x},\tau)$ is the P_ν density and $T^i{}_\nu(\boldsymbol{x},\tau)$ is the P_ν flux density. For $\nu \in \{1,2,3\}$ this equation describes a net change of momentum in the region:

$$\boldsymbol{F}_V(\tau) \equiv -\frac{\mathrm{d}}{\mathrm{d}\tau}\left[\boldsymbol{P}_V(\tau)\right] = -\hat{e}_j \oint_{\partial V} \mathrm{d}A_i \, T^i{}_j(\boldsymbol{x},\tau) \,. \tag{14}$$

Since momentum is leaving (or entering) the region V, this will be felt by the region's surroundings as a force $\boldsymbol{F}_V(\tau)$, exerted *by* the region, which would be measured for instance by a hypothetical pressure gauge placed at the boundary ∂V. Accordingly, $-\hat{e}_j T^i{}_j(\boldsymbol{x},\tau)$ is a force per unit area on a surface with a unit normal $\hat{e}_i$, and thus has a straightforward interpretation as a pressure. More generally, $-T^i{}_j(\boldsymbol{x},\tau)$ is referred to as the stress tensor, and encodes the pressures that would be measured on a surface in any orientation.

For a system in equilibrium, one will have zero net force exerted by any region V, and thus equal fluxes of momentum into and out of any region. In integral form, the equilibrium condition is:

$$\hat{e}_j \oint_{\partial V} \mathrm{d}A_i \, T^i{}_j(\boldsymbol{x},\tau) = 0 \,, \tag{15}$$

but the divergence theorem can be used to require this in differential form:

$$\partial_i T^i{}_j(\boldsymbol{x},\tau) = 0 \,. \tag{16}$$

This is possible even when $T^i{}_j(\boldsymbol{x},\tau) \neq 0$. If the stress tensor is non-zero in an equilibrium system, this means that static pressures will be felt, and in general the pressures will be anisotropic. The components of $S^{ij}(\boldsymbol{x},\tau) \equiv -T^i{}_j(\boldsymbol{x},\tau)$ are referred to as stresses and $S^{ij}(\boldsymbol{x},\tau)$ itself as the stress tensor, and these have an interpretation as furnishing mechanical pressures in a variety of continuum systems [51, 53, 55, 56], including fluids [52], solids [57], liquid crystals [58–60], and neutron stars [54, 61]. (See also Ref. [62] for a unified treatment of liquids, crystals, and liquid crystals.) Since the fundamental ontological objects of quantum field theory are fields rather than particles, it is sensible to interpret QCD as a theory of a continuous medium as well, and to interpret components of the operator $-\hat{T}^i{}_j(x)$ as stresses in this medium.

Although the mixed upper-lower form of the EMT has the most straightforward interpretation in terms of energy-momentum four-currents, it is convenient to work with tensors having all upper indices. The rules for raising and lowering indices in Eq. (A3) can be used to rewrite the energy-momentum four-currents entirely in terms of $T^{\mu\nu}(x)$. In light of this, the following dictionary can be quickly consulted to ascribe physical meanings to components of the EMT in tilted coordinates:

- **Energy density**:

$$\mathcal{E}(x) = T^0{}_0(x) = T^{00}(x) - T^{03}(x) \tag{17a}$$

- **Energy flux density**:

$$\boldsymbol{\mathcal{F}}_E(x) = T^i{}_0(x)\hat{e}_i = \big(T^{i0}(x) - T^{i3}(x)\big)\hat{e}_i \tag{17b}$$

- **Momentum density**:

$$\boldsymbol{\mathcal{P}}(x) = -T^0{}_i(x)\hat{e}_i = T^{01}(x)\hat{e}_x + T^{02}(x)\hat{e}_y + T^{00}(x)\hat{e}_z \tag{17c}$$

- **Stress tensor** (i.e., momentum flux densities):

$$S^{ij}(x) = -T^i{}_j(x) = T^{i1}(x)\delta^{j1} + T^{i2}(x)\delta^{j2} + T^{i0}(x)\delta^{j3} \tag{17d}$$

III. CONVOLUTION FORMALISM FOR PHYSICAL CURRENTS

In our previous work [33], we suggested that physical relativistic densities be identified as expectation values of local currents for physical states. If a physical state is described by a density matrix $\hat{\rho}$ (which is equal to $|\Psi\rangle\langle\Psi|$ for a pure state), this expectation value can written (in the Heisenberg picture):

$$\langle J^\mu(x)\rangle = \mathrm{Tr}\big[\hat{\rho}\hat{J}^\mu(x)\big] \xrightarrow[\text{pure state}]{} \langle\Psi|\hat{J}^\mu(x)|\Psi\rangle \,. \tag{18}$$

The central idea of Ref. [33] is that if the density is considered at fixed *light front time* τ rather than fixed Minkowski time, and if the longitudinal coordinate is integrated out, then the physical density can be written in terms of a state-independent internal density smeared out in a convolution relation. For a target without spin:

$$\langle J^\mu(\boldsymbol{x},\tau)\rangle_{2\mathrm{D}} \equiv \int \mathrm{d}x^3 \, \langle J^\mu(x)\rangle = \int \mathrm{d}^3\boldsymbol{R} \, \mathscr{P}^\mu{}_\nu(\boldsymbol{R},\tau) j^\nu(\boldsymbol{x}_\perp - \boldsymbol{R}_\perp) \,, \tag{19}$$

where $j^{\nu}(\boldsymbol{x}_\perp - \boldsymbol{R}_\perp)$ is the internal density and $\mathscr{P}^{\mu}{}_{\nu}(\boldsymbol{R},\tau)$ is the smearing function. The very possibility of this breakdown requires the use of light front synchronization, as proved in Appendix B of Ref. [33].

This relation should generalize in a straightforward way to the energy-momentum tensor:

$$\langle T^{\mu}{}_{\nu}(\boldsymbol{x},\tau)\rangle_{\text{2D}} = \int \mathrm{d}x^3\, \mathrm{Tr}\big[\hat{\rho}\hat{T}^{\mu}{}_{\nu}(x)\big] = \int \mathrm{d}^3\boldsymbol{R}\, \mathscr{Q}^{\mu}{}_{\alpha\nu}{}^{\beta}(\boldsymbol{R},\tau) t^{\alpha}{}_{\beta}(\boldsymbol{x}_\perp - \boldsymbol{R}_\perp)\,, \tag{20}$$

where here $t^{\alpha}{}_{\beta}(\boldsymbol{x}_\perp - \boldsymbol{R}_\perp)$ is the intrinsic EMT and $\mathscr{Q}^{\mu}{}_{\alpha\nu}{}^{\beta}(\boldsymbol{R},\tau)$ is the smearing function. (The generalization to targets with spin can be accomplished by replacing the densities and smearing functions with spin matrices, and including a trace in the convolution relation.)

A matter not addressed in our prior work [33] was how to systematically separate the smearing functions and internal densities. In fact, the separation is not unique. For a rather silly example of this, a factor 2 can be absorbed into $j^{\nu}(\boldsymbol{x}_\perp - \boldsymbol{R}_\perp)$ and a factor $\frac{1}{2}$ into $\mathscr{P}^{\mu}{}_{\nu}(\boldsymbol{R},\tau)$ without affecting the validity of Eq. (19). In this example, the alternative breakdown would produce an "internal density" that violates the charge sum rule, but more subtle alternative breakdowns could be formulated by adding a total divergence to the integrand in Eq. (19) or Eq. (20).

Although these breakdowns are not unique, we can formulate a reasonable systematic scheme for isolating the internal densities. In this scheme, we first construct classical analogues of Eqs. (19) and (20), in which the right-hand sides are effectively phase space functions of the target's position $\boldsymbol{r}$ and momentum $\boldsymbol{p}$. The analogue is explicitly constructed in Sec. III A for the four-current. We subsequently quantize the classical convolution to promote $\boldsymbol{r}$ and $\boldsymbol{p}$ to operators in Sec. III B. We will see that this gives us a fixed scheme for determining the rest-frame densities appearing in Eqs. (19) and (20), with the results appearing in Eqs. (41) and (43).

A. A classical analogy

Classically, the four-current of a stationary system (which is at rest at the origin) can be written $j^{\mu}_{\text{3D}}(\boldsymbol{x})$. The two-dimensional reduction is:

$$j^{\mu}_{\text{2D}}(\boldsymbol{x}_\perp) \equiv j^{\mu}(\boldsymbol{x}_\perp) = \int \mathrm{d}x^3\, j^{\mu}_{\text{3D}}(\boldsymbol{x})\,, \tag{21}$$

where we drop the 2D subscript for the reduced density since this is the desired quantity. We boost and translate the system in the following manner: (1) a longitudinal boost of rapidity η, (2) a transverse light front boost of velocity $\boldsymbol{\beta}_\perp$, and (3) a spatial translation by $\bar{r} = (0;\boldsymbol{r})$. We let $\Lambda^{\mu}{}_{\nu}$ signify the combined boost; an explicit formula is given in Eq. (A15). The 2D current becomes:

$$j^{\mu}(\boldsymbol{x}_\perp) \to J^{\mu}(\boldsymbol{x}_\perp;\boldsymbol{r},\boldsymbol{p}) = \Lambda^{\mu}{}_{\nu} \int \mathrm{d}(\Lambda x)^3\, j^{\nu}_{\text{3D}}(\Lambda^{-1}[x-\bar{r}]) = \mathrm{e}^{-\eta}\Lambda^{\mu}{}_{\nu} j^{\nu}(\Lambda^{-1}[x-\bar{r}])\,, \tag{22}$$

where the factor $\mathrm{e}^{-\eta}$ comes from $\mathrm{d}(\Lambda x)^3 = \mathrm{e}^{-\eta}\,\mathrm{d}x^3$. It is worth remarking that although $j^{\nu}(\Lambda^{-1}[x-\bar{r}])$ depends only on the transverse spatial components of $\Lambda^{-1}[x-\bar{r}]$, it obtains a dependence on the light front time $\tau = x^0$ through these.

If we are ignorant of the exact position and momentum of the system, but have a phase space distribution $\rho(\boldsymbol{r},\boldsymbol{p};0)$ at $\tau=0$, we can still calculate an expectation value for the current through:

$$\langle J^{\mu}(\boldsymbol{x}_\perp,\tau)\rangle_{\text{2D}} = \int \mathrm{d}^3\boldsymbol{r} \int \mathrm{d}\mu(\boldsymbol{p})\, \rho(\boldsymbol{r},\boldsymbol{p};0)\, \mathrm{e}^{-\eta}\Lambda^{\mu}{}_{\nu} j^{\nu}(\Lambda^{-1}[x-\bar{r}])\,, \tag{23}$$

where $\mathrm{d}\mu(\boldsymbol{p})$ is a momentum integration element (the exact form of which doesn't matter here). The time dependence in $j^{\nu}(\Lambda^{-1}[x-\bar{r}])$ can be moved into the phase space distribution instead, by defining:

$$\rho(\boldsymbol{r},\boldsymbol{p};\tau) \equiv \mathrm{e}^{-(\boldsymbol{\beta}\cdot\boldsymbol{\nabla})\tau} \rho(\boldsymbol{r},\boldsymbol{p};0)\,, \tag{24}$$

and by replacing $\bar{r}$ with $r = (\tau;\boldsymbol{r})$ in the rest-frame current. One can think of this as a classical analogy of switching from the Heisenberg to the Schrödinger picture of quantum mechanics.

Because $x^0 = r^0$, the transverse components of $\Lambda^{-1}[x-r]$ are just $\boldsymbol{x}_\perp - \boldsymbol{r}_\perp$ (see Eq. (A15)) which is a manifestation of the Galilean subgroup of the Poincaré group. This allows the classical expectation value to be written:

$$\langle J^{\mu}(\boldsymbol{x}_\perp,\tau)\rangle_{\text{2D}} = \int \mathrm{d}^3\boldsymbol{r} \int \mathrm{d}\mu(\boldsymbol{p})\, \rho(\boldsymbol{r},\boldsymbol{p};\tau)\, \mathrm{e}^{-\eta}\Lambda^{\mu}{}_{\nu} j^{\nu}(\boldsymbol{x}_\perp - \boldsymbol{r}_\perp)\,. \tag{25}$$

This is the formula we shall proceed to quantize.

B. Quantization of the analogy

Quantization of Eq. (25) should take the form:

$$\langle J^\mu(\boldsymbol{x}_\perp,\tau)\rangle_{\text{2D}} = \mathrm{Tr}\Big[\hat\rho(\tau)\,\widehat{\mathrm{e}^{-\eta}\Lambda^\mu{}_\nu j^\nu(\boldsymbol{x}_\perp-\boldsymbol{r}_\perp)}\Big] \tag{26}$$

in the Schrödinger picture, where $\widehat{\mathrm{e}^{-\eta}\Lambda^\mu{}_\nu j^\nu(\boldsymbol{x}_\perp-\boldsymbol{r}_\perp)}$ is an operator corresponding to the classical $\mathrm{e}^{-\eta}\Lambda^\mu{}_\nu j^\nu(\boldsymbol{x}_\perp-\boldsymbol{r}_\perp)$. It is well-known that there is not a unique map from classical phase space functions to quantum-mechanical operators [63, 64], so there is some freedom in how to choose the appropriate operator. We choose the following operator:

$$\widehat{\mathrm{e}^{-\eta}\Lambda^\mu{}_\nu j^\nu(\boldsymbol{x}_\perp-\boldsymbol{r}_\perp)} = \frac{1}{2}\frac{m}{\hat P_z}\Big\{\Lambda^\mu{}_\nu(\hat{\boldsymbol{P}}),\, j^\nu(\boldsymbol{x}_\perp-\hat{\boldsymbol{R}}_\perp)\Big\}\,, \tag{27}$$

where $\{\cdot,\cdot\}$ is the anticommutator and where $\eta=\log(p_z/m)$ was used. This operator is Hermitian, as required, and has the benefit of being fairly simple. If this operator is sandwiched between momentum kets, it gives:

$$\left\langle \boldsymbol{p}'\middle|\frac{1}{2}\frac{m}{\hat P_z}\Big\{\Lambda^\mu{}_\nu(\hat{\boldsymbol{P}}),\, j^\nu(\boldsymbol{x}_\perp-\hat{\boldsymbol{R}}_\perp)\Big\}\middle|\boldsymbol{p}\right\rangle = \frac{1}{2}\Big(\Lambda^\mu{}_\nu(\boldsymbol{p})+\Lambda^\mu{}_\nu(\boldsymbol{p}')\Big)\frac{m}{p_z}\langle\boldsymbol{p}'|j^\nu(\boldsymbol{x}_\perp-\hat{\boldsymbol{R}}_\perp)|\boldsymbol{p}\rangle\,. \tag{28}$$

Note that this matrix element is zero if $p'_z\neq p_z$. We will denote the average of the two Lorentz boost matrices appearing here as:

$$\bar\Lambda^\mu{}_\nu \equiv \frac{1}{2}\Big(\Lambda^\mu{}_\nu(\boldsymbol{p})+\Lambda^\mu{}_\nu(\boldsymbol{p}')\Big)\,, \tag{29}$$

which as a 4×4 matrix it can be written:

$$\bar\Lambda^\mu{}_\nu = \begin{bmatrix} P_z/m & 0 & 0 & 0\\ P_x/m & 1 & 0 & 0\\ P_y/m & 0 & 1 & 0\\ (P_z-P_0)/m & -P_x/P_z & -P_y/P_z & m/P_z\end{bmatrix}\,. \tag{30}$$

Here $P=\frac{1}{2}\big(p+p'\big)$ is the average of the initial and final kets' four-momenta. It should be noted that $\bar\Lambda^\mu{}_\nu$ is not a Lorentz transform, since Lorentz transforms are not closed under addition[1], and we define it as the average of two boosts. In particular, $\bar\Lambda^\mu{}_\nu$ does not preserve the metric (as explicitly shown in Appendix B). This is not an issue for us since $\bar\Lambda^\mu{}_\nu$ simply encodes the momentum dependence of a matrix element and is not being used (in the quantum-mechanical context) to parametrize boosts of matrix elements. However, the fact that $\bar\Lambda^\mu{}_\nu$ is not a Lorentz transform should be kept in mind when performing mathematical manipulations, so that operations that are valid for Lorentz transforms are not used uncritically.

With the quantization map defined, we can proceed. In terms of the tensor $\bar\Lambda^\mu{}_\nu$, we can write momentum-ket matrix elements as:

$$\langle\boldsymbol{p}'|\widehat{\mathrm{e}^{-\eta}\Lambda^\mu{}_\nu j^\nu(\boldsymbol{x}_\perp-\boldsymbol{r}_\perp)}|\boldsymbol{p}\rangle = \frac{m}{p_z}\bar\Lambda^\mu{}_\nu\langle\boldsymbol{p}'|j^\nu(\boldsymbol{x}_\perp-\hat{\boldsymbol{R}}_\perp)|\boldsymbol{p}\rangle\,. \tag{31}$$

The completeness relation

$$\int\frac{\mathrm{d}^3\boldsymbol{p}}{2p_z(2\pi)^3}|\boldsymbol{p}\rangle\langle\boldsymbol{p}| = 1 \tag{32}$$

can be inserted twice into Eq. (26), and when Eq. (31) is used, we obtain:

$$\langle J^\mu(\boldsymbol{x}_\perp,\tau)\rangle_{\text{2D}} = \int\frac{\mathrm{d}^3\boldsymbol{p}}{2p_z(2\pi)^3}\int\frac{\mathrm{d}^3\boldsymbol{p}'}{2p'_z(2\pi)^3}\frac{m}{p_z}\bar\Lambda^\mu{}_\nu\langle\boldsymbol{p}|\hat\rho(\tau)|\boldsymbol{p}'\rangle\langle\boldsymbol{p}'|j^\nu(\boldsymbol{x}_\perp-\hat{\boldsymbol{R}}_\perp)|\boldsymbol{p}\rangle\,, \tag{33}$$

where $\bar\Lambda^\mu{}_\nu$ is as given in Eq. (30). The remaining operator dependence can be eliminated using transverse position eigenkets. Since the transformation properties of the transverse plane are Galilean, these properties mirror the properties of non-relativistic kets:

$$\langle\boldsymbol{R}_\perp|\boldsymbol{R}'_\perp\rangle = \delta^{(2)}(\boldsymbol{R}_\perp-\boldsymbol{R}'_\perp) \tag{34a}$$

$$\int\mathrm{d}^2\boldsymbol{R}_\perp\,|\boldsymbol{R}_\perp\rangle\langle\boldsymbol{R}_\perp| = 1 \tag{34b}$$

$$\langle\boldsymbol{p}_\perp|\boldsymbol{R}_\perp\rangle = \mathrm{e}^{-\mathrm{i}\boldsymbol{p}_\perp\cdot\boldsymbol{R}_\perp}\,. \tag{34c}$$

[1] Formally, Lorentz transforms form a group under multiplication, but do not form a ring.

Understanding that $|\boldsymbol{p}\rangle = |p_z\rangle \otimes |\boldsymbol{p}_\perp\rangle$, inserting Eq. (34b) into Eq. (33) and using Eq. (34c) gives:

$$\langle J^\mu(\boldsymbol{x}_\perp,\tau)\rangle_{2\mathrm{D}} = \int \mathrm{d}^2\boldsymbol{R}_\perp \int \mathrm{d}^2\boldsymbol{R}'_\perp \int \frac{\mathrm{d}^3\boldsymbol{p}}{2p_z(2\pi)^3} \int \frac{\mathrm{d}^3\boldsymbol{p}'}{2p'_z(2\pi)^3} \frac{m}{p_z} \bar{\Lambda}^\mu{}_\nu \langle \boldsymbol{p}|\hat{\rho}(\tau)|\boldsymbol{p}'\rangle \\ \times j^\nu(\boldsymbol{x}_\perp - \boldsymbol{R}_\perp)\langle \boldsymbol{R}'_\perp|\boldsymbol{R}_\perp\rangle\langle p'_z|p_z\rangle\, \mathrm{e}^{-\mathrm{i}(\boldsymbol{p}'_\perp\cdot\boldsymbol{R}'_\perp - \boldsymbol{p}_\perp\cdot\boldsymbol{R}_\perp)}\,. \tag{35}$$

Using Eq. (34a) and $\langle p'_z|p_z\rangle = 2p_z(2\pi)\delta(p_z - p'_z)$ reduces this to:

$$\langle J^\mu(\boldsymbol{x}_\perp,\tau)\rangle_{2\mathrm{D}} = \int \mathrm{d}^2\boldsymbol{R}_\perp \int \frac{\mathrm{d}p_z}{2p_z(2\pi)} \int \frac{\mathrm{d}^2\boldsymbol{p}_\perp}{(2\pi)^2} \int \frac{\mathrm{d}^2\boldsymbol{p}'_\perp}{(2\pi)^2} \frac{m}{p_z} \bar{\Lambda}^\mu{}_\nu \langle \boldsymbol{p}|\hat{\rho}(\tau)|\boldsymbol{p}'\rangle j^\nu(\boldsymbol{x}_\perp - \boldsymbol{R}_\perp)\, \mathrm{e}^{-\mathrm{i}(\boldsymbol{p}'_\perp - \boldsymbol{p}_\perp)\cdot\boldsymbol{R}_\perp}\,. \tag{36}$$

Finally, changing variables to $P = \frac{1}{2}\big(p + p'\big)$ and $\Delta = p' - p$ gives:

$$\langle J^\mu(\boldsymbol{x}_\perp,\tau)\rangle_{2\mathrm{D}} = \int \mathrm{d}^2\boldsymbol{R}_\perp \int \frac{\mathrm{d}^3\boldsymbol{P}}{2P_z(2\pi)^3} \int \frac{\mathrm{d}^2\boldsymbol{\Delta}_\perp}{(2\pi)^2} \frac{m}{P_z} \bar{\Lambda}^\mu{}_\nu \langle \boldsymbol{p}|\hat{\rho}(\tau)|\boldsymbol{p}'\rangle j^\nu(\boldsymbol{x}_\perp - \boldsymbol{R}_\perp)\, \mathrm{e}^{-\mathrm{i}\boldsymbol{\Delta}_\perp\cdot\boldsymbol{R}_\perp}\,. \tag{37}$$

This is sufficient to determine that the integrated smearing function appearing in Eq. (19) is:

$$\int \mathrm{d}R_z\, \mathscr{P}^\mu{}_\nu(\boldsymbol{R},\tau) = \int \frac{\mathrm{d}^3\boldsymbol{P}}{2P_z(2\pi)^3} \int \frac{\mathrm{d}^2\boldsymbol{\Delta}_\perp}{(2\pi)^2} \frac{m}{P_z} \bar{\Lambda}^\mu{}_\nu \langle \boldsymbol{p}|\hat{\rho}(\tau)|\boldsymbol{p}'\rangle\, \mathrm{e}^{-\mathrm{i}\boldsymbol{\Delta}_\perp\cdot\boldsymbol{R}_\perp}\,, \tag{38}$$

though we will not concern ourselves further with explicit evaluation of this expression or reconstruction of the R_z dependence.

Instead, the crucial matter at hand is to relate the internal, rest-frame density $j^\nu(\boldsymbol{x}_\perp - \boldsymbol{R}_\perp)$ to the field-theoretic matrix element $\langle \boldsymbol{p}'|\hat{J}^\mu(0)|\boldsymbol{p}\rangle$. To do this, we write the 2D expectation value of the current in the Schödinger picture as:

$$\langle J^\mu(\boldsymbol{x}_\perp,\tau)\rangle_{2\mathrm{D}} = \int \mathrm{d}x^3 \mathrm{Tr}\Big[\hat{\rho}(\tau)\,\hat{J}^\mu(\boldsymbol{x})\Big] = \int \frac{\mathrm{d}^3\boldsymbol{P}}{2P_z(2\pi)^3} \int \frac{\mathrm{d}^2\boldsymbol{\Delta}_\perp}{(2\pi)^2} \langle \boldsymbol{p}|\hat{\rho}(\tau)|\boldsymbol{p}'\rangle \frac{\langle \boldsymbol{p}'|\hat{J}^\mu(0)|\boldsymbol{p}\rangle}{2P_z}\, \mathrm{e}^{-\mathrm{i}\boldsymbol{\Delta}_\perp\cdot\boldsymbol{x}_\perp}\bigg|_{\Delta_z=0}\,. \tag{39}$$

Comparing to Eq. (37) and requiring these expressions for the physical current to be identical for all choices of $\hat{\rho}(\tau)$ requires that:

$$\frac{m}{P_z}\bar{\Lambda}^\mu{}_\nu j^\nu(\boldsymbol{x}_\perp - \boldsymbol{R}_\perp)\, \mathrm{e}^{-\mathrm{i}\boldsymbol{\Delta}_\perp\cdot\boldsymbol{R}_\perp} = \frac{\langle \boldsymbol{p}'|\hat{J}^\mu(0)|\boldsymbol{p}\rangle}{2P_z}\, \mathrm{e}^{-\mathrm{i}\boldsymbol{\Delta}_\perp\cdot\boldsymbol{x}_\perp}\,, \tag{40}$$

which can be inverted to find:

$$j^\mu(\boldsymbol{b}_\perp) = \int \frac{\mathrm{d}^2\boldsymbol{\Delta}_\perp}{(2\pi)^2} (\bar{\Lambda}^{-1})^\mu{}_\nu \frac{\langle \boldsymbol{p}'|\hat{J}^\nu(0)|\boldsymbol{p}\rangle}{2m}\, \mathrm{e}^{-\mathrm{i}\boldsymbol{\Delta}_\perp\cdot\boldsymbol{b}_\perp}\,, \tag{41}$$

where $\boldsymbol{b}_\perp = \boldsymbol{x}_\perp - \boldsymbol{R}_\perp$ is the impact parameter. This is our ultimate expression for the internal, rest-frame current of a spin-zero target. For spin-half targets, this is generalized by introducing light front helicity indices λ, λ' into the kets.

The rationale for arriving at Eq. (41) can be extended in a straightforward way to the EMT. The primary difference is that there are two Lorentz indices, so an additional Lorentz boost matrix must be applied in the classical expression. When quantizing an expression with two Lorentz boosts, the anticommutator is taken twice:

$$\overline{\mathrm{e}^{-\eta}\Lambda^\mu{}_\alpha\Lambda_\nu{}^\beta t^\alpha{}_\beta(\boldsymbol{x}_\perp - \boldsymbol{r}_\perp)} = \frac{1}{4}\frac{m}{\hat{P}_z}\Big\{\Lambda^\mu{}_\alpha(\hat{\boldsymbol{P}}),\, \big\{\Lambda_\nu{}^\beta(\hat{\boldsymbol{P}}),\, t^\alpha{}_\beta(\boldsymbol{x}_\perp - \hat{\boldsymbol{R}}_\perp)\big\}\Big\}\,. \tag{42}$$

When worked out, the result for the intrinsic, rest-frame EMT (with helicity indices included) is:

$$t^\mu{}_\nu(\boldsymbol{b}_\perp;\lambda,\lambda') = \int \frac{\mathrm{d}^2\boldsymbol{\Delta}_\perp}{(2\pi)^2} (\bar{\Lambda}^{-1})^\mu{}_\alpha (\bar{\Lambda}^{-1})_\nu{}^\beta \frac{\langle \boldsymbol{p}',\lambda'|\hat{T}^\alpha{}_\beta(0)|\boldsymbol{p},\lambda\rangle}{2m}\, \mathrm{e}^{-\mathrm{i}\boldsymbol{\Delta}_\perp\cdot\boldsymbol{b}_\perp}\,. \tag{43}$$

It is this formula that we will apply for the remainder of the main body of this work.

IV. ENERGY-MOMENTUM TENSOR OF SPIN-ZERO TARGETS

Although we are primarily interested in the proton in this work, we consider spin-zero target first as a warm-up exercise, since the resulting densities are simpler and already contain subtleties to address.

The standard form factor breakdown for the EMT of a spin-zero target is [15]:

$$\langle \boldsymbol{p}' | \hat{T}^{\mu\nu}(0) | \boldsymbol{p} \rangle = 2P^\mu P^\nu A(\varDelta^2) + \frac{1}{2}\Big(\varDelta^\mu \varDelta^\nu - \varDelta^2 g^{\mu\nu}\Big) D(\varDelta^2)\,. \tag{44}$$

When $\varDelta_z = 0$, Eqs. (B9) and (B11) can be used to find:

$$(\bar{\varLambda}^{-1})^\mu{}_\alpha (\bar{\varLambda}^{-1})^\nu{}_\beta \frac{\langle \boldsymbol{p}' | \hat{T}^{\alpha\beta}(0) | \boldsymbol{p} \rangle}{2m} = m \left\{ \bar{n}^\mu \bar{n}^\nu A(-\boldsymbol{\varDelta}_\perp^2) + \left(\frac{\varDelta_\perp^\mu \varDelta_\perp^\nu + \boldsymbol{\varDelta}_\perp^2 g^{\mu\nu}}{4m^2} \right) D(-\boldsymbol{\varDelta}_\perp^2) - \left(\frac{\boldsymbol{\varDelta}_\perp^2}{4m^2} \right)^2 n^\mu n^\nu D(-\boldsymbol{\varDelta}_\perp^2) \right\}. \tag{45}$$

According to Eq. (43), the intrinsic, rest-frame EMT of the spin-zero hadron is given by the Fourier transform of this quantity. The interpretations of individual components of the EMT were described in Sec. II; we shall presently analyze results for the components in terms of those interpretations.

A. Energy density

Consulting the dictionary of Eq. (17), the rest frame energy density for a spin-zero target is:

$$\mathcal{E}(\boldsymbol{b}_\perp) = t^{00}(\boldsymbol{b}_\perp) - t^{03}(\boldsymbol{b}_\perp) = m \int \frac{\mathrm{d}^2\boldsymbol{\varDelta}_\perp}{(2\pi)^2} \left(A(-\boldsymbol{\varDelta}_\perp^2) + \frac{\boldsymbol{\varDelta}_\perp^2}{4m^2} D(-\boldsymbol{\varDelta}_\perp^2) \right) \mathrm{e}^{-\mathrm{i}\boldsymbol{\varDelta}_\perp \cdot \boldsymbol{b}_\perp}\,. \tag{46}$$

This is a new result. Although a prior results exist for energy densities of spin-zero [31] and spin-half [16] targets in standard light front coordinates, the tilted coordinate energy is different from the light front energy, so naturally Eq. (46) differs from the light front energy density in Ref. [31]. In fact, the energy in tilted light front coordinates is equal to the more familiar instant form energy [33], for which Eq. (46) provides a two-dimensional relativistic density in the target's rest frame.

Integrating Eq. (46) gives m as the total energy, as expected for a system at rest. Additionally, Eq. (46) can be used to define a rest-frame energy radius:

$$\langle \boldsymbol{b}_\perp^2 \rangle_{\text{energy}} \equiv \frac{1}{m} \int \mathrm{d}^2\boldsymbol{b}_\perp\, \boldsymbol{b}_\perp^2\, \mathcal{E}(\boldsymbol{b}_\perp) = 4 \frac{\mathrm{d}A(\varDelta^2)}{\mathrm{d}\varDelta^2}\bigg|_{\varDelta^2=0} - \frac{1}{m^2} D(0)\,. \tag{47}$$

This radius is notably not zero for pointlike particles. Since $D_{\text{free}}(\varDelta^2) = -1$ [15], the free spin-zero boson an energy radius of $1/(2m)$.

Although $D_{\text{free}}(\varDelta^2) = -1$ follows naturally for Klein-Gordon fields by applying Noether's theorems [65] or by differentiating the action with respect to the metric [15], we might wonder how the energy radius would differ if $D_{\text{free}}(\varDelta^2)$ were a different constant. In fact, several authors [15, 29, 66] argue that the EMT is only defined up to a trivially conserved quantity, and that the form factor $D(\varDelta^2)$ can be altered by adding such a quantity. However, Eq. (47) will only give a non-negative squared radius if:

$$D_{\text{free}}(0) \leq 0\,. \tag{48}$$

The negativity of $D(0)$ has previously been postulated by Polyakov [15, 67] as a mechanical stability criterion. Within the context of an energy radius, however, this constraint can be relaxed for composite particles, since $A(\varDelta^2)$ is no longer constant. More generally, the criterion of positive squared radius imposes:

$$D(0) \leq 4m^2 \frac{\mathrm{d}A(\varDelta^2)}{\mathrm{d}\varDelta^2}\bigg|_{\varDelta^2=0}, \tag{49}$$

which may allow $D(0) > 0$ for composite particles, but still imposes a maximum value.

B. Momentum density

From the dictionary in Eq. (17), the momentum density is given by:

$$\boldsymbol{\mathcal{P}}(\boldsymbol{b}_\perp) = t^{01}(\boldsymbol{b}_\perp)\hat{e}_x + t^{02}(\boldsymbol{b}_\perp)\hat{e}_y + t^{00}(\boldsymbol{b}_\perp)\hat{e}_z = m\hat{e}_z \int \frac{\mathrm{d}^2\boldsymbol{\varDelta}_\perp}{(2\pi)^2} A(-\boldsymbol{\varDelta}_\perp^2)\, \mathrm{e}^{-\mathrm{i}\boldsymbol{\varDelta}_\perp \cdot \boldsymbol{b}_\perp}\,, \tag{50}$$

which is non-zero only for the longitudinal momentum. Significantly, the z momentum in tilted coordinates is equal to the plus momentum in light front coordinates: $P_z = P^+_{\text{LF}}$. It is thus not surprising that the momentum density we find is equal to prior results for the light front momentum density [17] upon setting $P^+_{\text{LF}} \to m$.

It is worth stressing (see Ref. [33] and Appendix A) that—in tilted coordinates—P_z is equal to m rather than 0 at rest. Thus, a non-zero P_z density does not indicate motion within the system. Rather than a density for a quantity of motion, the P_z density can be interpreted as an inertia density, since classically, contravariant components of the tilted momentum and the velocity are related by $p^i = p_z v^i$. On the other hand, the energy fluxes ${t^i}_0$ have a clearer interpretation as encoding motion within the system. We shall look at these next.

C. Energy flux density

From the dictionary in Eq. (17), the energy flux density is given by:

$$\boldsymbol{\mathcal{F}}_E(\boldsymbol{b}_\perp) = \big(t^{i0}(\boldsymbol{b}_\perp) - t^{i3}(\boldsymbol{b}_\perp)\big)\hat{e}_i = m\hat{e}_z \int \frac{\mathrm{d}^2\boldsymbol{\Delta}_\perp}{(2\pi)^2} \left(\frac{\boldsymbol{\Delta}_\perp^2}{4m^2}\right)^2 D(-\boldsymbol{\Delta}_\perp^2)\,. \tag{51}$$

Surprisingly, for a spin-zero target at rest, there appears (within this framework) to be a non-zero energy flux density in the z direction. Since the spin-zero target does not intrinsically single out any direction, and the z direction is only special because of its appearance in the time synchronization convention, this non-zero energy flux must be synchronization-induced, much like the azimuthal modulations in spin-half charge densities [33]. The emergence of the synchronization-induced energy flux is explored by using a toy model in Sec. IV E.

D. Stress tensor

Using the dictionary in Eq. (17), the stress tensor for a spin-zero target is:

$$S^{ij}(\boldsymbol{b}_\perp) = t^{i1}\delta^{j1} + t^{i2}\delta^{j2} + t^{i0}\delta^{j3} = \frac{1}{4m}\int \frac{\mathrm{d}^2\boldsymbol{\Delta}_\perp}{(2\pi)^2}\Big(\Delta_\perp^i\Delta_\perp^j - \delta^{ij}\boldsymbol{\Delta}_\perp^2\Big) D(-\boldsymbol{\Delta}_\perp^2)\,\mathrm{e}^{-\,\mathrm{i}\boldsymbol{\Delta}_\perp\cdot\boldsymbol{b}_\perp}\,. \tag{52}$$

The transverse components $i,j \in \{1,2\}$ of the stress tensor by themselves reproduce prior results for the transverse light front stress tensor [17] if one sets $P^+_{\text{LF}} \to m$.

More remarkably, however, there is apparently a new longitudinal pressure:

$$p_z(\boldsymbol{b}_\perp) \equiv S^{33}(\boldsymbol{b}_\perp) = -\int \frac{\mathrm{d}^2\boldsymbol{\Delta}_\perp}{(2\pi)^2}\frac{\boldsymbol{\Delta}_\perp^2}{4m} D(-\boldsymbol{\Delta}_\perp^2)\,\mathrm{e}^{-\,\mathrm{i}\boldsymbol{\Delta}_\perp\cdot\boldsymbol{b}_\perp}\,, \tag{53}$$

where, as is standard in continuum mechanics [51–53, 55–57], normal stresses are called pressures. Shear stresses involving the z direction, which would correspond to fluxes of P_z in the transverse plane or longitudinal fluxes of $\boldsymbol{P}_\perp$, vanish for the spin-zero target. This is likely a consequence of the z coordinate dependence being integrated out, as integrating out x or y likewise leads to the elimination of shear stresses in integrated-out direction.

E. Toy model for synchronization-induced energy flux

We next construct a simple toy model to understand how using light front synchronization can induce an apparent energy flux where none would appear under Einstein synchronization.

In this toy model, we imagine an outward-going shell of energy and an inward-coming shell of equal energy situated around a point at the origin. This model is illustrated in Fig. 2, and this situation is assumed to hold at an Einstein (instant form) time $t = 0$. We will ultimately take both the shell thickness and radius to zero in order to analyze the energy flux and static pressure at a point, but keep these finite in the course of the derivation. At angles (θ, ϕ) and Einstein time $t \approx 0$, the radial coordinate of the outgoing and incoming shell are respectively:

$$\boldsymbol{r}_{\text{O}}(\theta,\phi;t) = (R+vt)\big\{\hat{e}_z\cos\theta + \hat{e}_x\sin\theta\cos\phi + \hat{e}_y\sin\theta\sin\phi\big\} \tag{54a}$$

$$\boldsymbol{r}_{\text{I}}(\theta,\phi;t) = (R+h-vt)\big\{\hat{e}_z\cos\theta + \hat{e}_x\sin\theta\cos\phi + \hat{e}_y\sin\theta\sin\phi\big\} \tag{54b}$$

where v is the magnitude of the instant form velocity of the shell and h is the shell thickness. Eq. (54) defines the toy model.

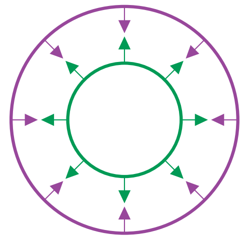

FIG. 2. Pictorial representation of the toy model, in one a spherical shell of incoming energy moves towards the origin (purple) and another shell of outgoing energy moves away from the origin (green).

Under Einstein synchronization (i.e., instant form coordinates), the instantaneous velocities (at $t = 0$) are:

$$\boldsymbol{v}_{\mathrm{O}}^{(\mathrm{IF})}(\theta,\phi) = +v\big\{\hat{e}_z\cos\theta + \hat{e}_x\sin\theta\cos\phi + \hat{e}_y\sin\theta\sin\phi\big\} \tag{55a}$$

$$\boldsymbol{v}_{\mathrm{I}}^{(\mathrm{IF})}(\theta,\phi) = -v\big\{\hat{e}_z\cos\theta + \hat{e}_x\sin\theta\cos\phi + \hat{e}_y\sin\theta\sin\phi\big\}\,, \tag{55b}$$

where we are explicitly signifying the instant form velocities with a superscript, and the energy flux through the shell at these angles is:

$$\boldsymbol{\mathcal{F}}_E^{(\mathrm{IF})}(\theta,\phi) = \big(\boldsymbol{v}_{\mathrm{O}}^{(\mathrm{IF})}(\theta,\phi) + \boldsymbol{v}_{\mathrm{I}}^{(\mathrm{IF})}(\theta,\phi)\big)\varepsilon = 0\,, \tag{56}$$

where ε is the energy density of the shell. Thus, under Einstein synchronization, there is no net energy flux.

Under light front synchronization, the trajectories of elements of the shell should be written as functions of light front time $\tau = t + z$ rather than Einstein time t, and we take the derivative with respect to the former taken to obtain velocities. The shell element positions, as functions of τ, are:

$$\boldsymbol{r}_{\mathrm{O}}(\theta,\phi;\tau) = \frac{(1 - v\cos\theta)R + v\tau}{1 + v\cos\theta}\big\{\hat{e}_z\cos\theta + \hat{e}_x\sin\theta\cos\phi + \hat{e}_y\sin\theta\sin\phi\big\} \tag{57a}$$

$$\boldsymbol{r}_{\mathrm{I}}(\theta,\phi;t) = \frac{(1 + v\cos\theta)(R + h) - v\tau}{1 - v\cos\theta}\big\{\hat{e}_z\cos\theta + \hat{e}_x\sin\theta\cos\phi + \hat{e}_y\sin\theta\sin\phi\big\}\,, \tag{57b}$$

and accordingly the instantaneous velocities at $\tau = 0$ are:

$$\boldsymbol{v}_{\mathrm{O}}(\theta,\phi) = +\frac{v}{1 + v\cos\theta}\big\{\hat{e}_z\cos\theta + \hat{e}_x\sin\theta\cos\phi + \hat{e}_y\sin\theta\sin\phi\big\} \tag{58a}$$

$$\boldsymbol{v}_{\mathrm{I}}(\theta,\phi) = -\frac{v}{1 - v\cos\theta}\big\{\hat{e}_z\cos\theta + \hat{e}_x\sin\theta\cos\phi + \hat{e}_y\sin\theta\sin\phi\big\}\,, \tag{58b}$$

Since tilted energy is equal to instant form energy, the energy flux through the shell at these angles is:

$$\boldsymbol{\mathcal{F}}_E(\theta,\phi) = \big(\boldsymbol{v}_{\mathrm{O}}(\theta,\phi) + \boldsymbol{v}_{\mathrm{I}}(\theta,\phi)\big)\varepsilon = -\frac{2v^2\cos\theta}{1 - v^2\cos^2\theta}\big\{\hat{e}_z\cos\theta + \hat{e}_x\sin\theta\cos\phi + \hat{e}_y\sin\theta\sin\phi\big\}\varepsilon\,, \tag{59}$$

which is non-zero. To shrink the shell to a point and obtain the energy flux at this point, we average the energy flux over all angles. Doing so gives:

$$\langle\boldsymbol{\mathcal{F}}_E\rangle_\Omega \equiv \frac{1}{4\pi}\int \mathrm{d}\Omega\, \boldsymbol{f}_E(\theta,\phi) = \varepsilon\hat{e}_z\left(1 - \frac{\tanh^{-1}(v)}{v}\right)\,. \tag{60}$$

As promised, we have shown that using light front synchronization can induce an energy flux where there was none under Einstein synchronization. This can occur specifically in cases where, under Einstein synchronization, there are equal and opposite fluxes of energy. In short, this occurs because light front synchronization is asymmetric in the z direction; the speed of light is infinite in the $-z$ direction but $c/2$ in the $+z$ direction, and more generally velocities that are equal and opposite under Einstein synchronization become unequal under light front synchronization. This can induce apparent z-direction fluxes.

V. ENERGY-MOMENTUM TENSOR OF SPIN-HALF TARGETS

Since our primary objective is to obtain energy-momentum densities and currents for the proton, we proceed to consider spin-half targets. We primarily focus on the symmetric Belinfante EMT, but will briefly consider how the formalism changes when the asymmetric EMT is instead used in Sec. V F.

The standard form factor breakdown for the symmetric EMT for spin-half targets is [15]:

$$\langle \boldsymbol{p}', \lambda' | \hat{T}^{\mu\nu}(0) | \boldsymbol{p}, \lambda \rangle = \bar{u}(\boldsymbol{p}', \lambda') \bigg\{ \frac{\gamma^{\{\mu} P^{\nu\}}}{2} A(\Delta^2) + \frac{\mathrm{i} P^{\{\mu} \sigma^{\nu\}\rho} \Delta_\rho}{4m} B(\Delta^2) + \frac{\Delta^\mu \Delta^\nu - g^{\mu\nu}\Delta^2}{4m} D(\Delta^2) \bigg\} u(\boldsymbol{p}, \lambda) \,. \tag{61}$$

Using formulas from Appendix A of Ref. [33], we can explicitly evaluate matrix elements of the EMT when $\Delta_z = 0$ to be:

$$\begin{aligned} \langle \boldsymbol{p}', \lambda' | \hat{T}^{\mu\nu}(0) | \boldsymbol{p}, \lambda \rangle = 2 P^\mu P^\nu & \left\{ (\sigma_0)_{\lambda'\lambda} A(-\boldsymbol{\Delta}_\perp^2) - \frac{\mathrm{i}\epsilon^{\alpha\beta\gamma\delta} n_\alpha \bar{n}_\beta \Delta_\gamma (\sigma_\delta)_{\lambda'\lambda}}{2m} B(-\boldsymbol{\Delta}_\perp^2) \right\} \\ & + \left\{ - \frac{\mathrm{i} P^{\{\mu} \epsilon^{\nu\}\rho\sigma\tau} n_\rho P_\sigma \Delta_\tau}{(P\cdot n)} (\sigma_3)_{\lambda'\lambda} + \frac{m P^{\{\mu} n^{\nu\}}}{(P\cdot n)} \mathrm{i}\epsilon^{\alpha\beta\gamma\delta} n_\alpha \bar{n}_\beta \Delta_\gamma (\sigma_\delta)_{\lambda'\lambda} \right\} J(-\boldsymbol{\Delta}_\perp^2) \\ & + \frac{\Delta^\mu\Delta^\nu - g^{\mu\nu}\Delta^2}{2} \left((\sigma_0)_{\lambda'\lambda} + \frac{\mathrm{i}\epsilon^{\alpha\beta\gamma\delta} n_\alpha \bar{n}_\beta \Delta_\gamma (\sigma_\delta)_{\lambda'\lambda}}{2m} \right) D(-\boldsymbol{\Delta}_\perp^2) \,, \end{aligned} \tag{62}$$

where

$$J(\Delta^2) = \frac{1}{2}\big(A(\Delta^2) + B(\Delta^2) \big) \tag{63}$$

is the angular momentum form factor [15]. Further using the formulas in Appendix B, it can be shown that:

$$\begin{aligned} (\bar{\Lambda}^{-1})^\mu{}_\alpha (\bar{\Lambda}^{-1})^\nu{}_\beta \frac{\langle \boldsymbol{p}', \lambda' | \hat{T}^{\alpha\beta}(0) | \boldsymbol{p}, \lambda \rangle}{2m} = m \bar{n}^\mu \bar{n}^\nu & \left\{ (\sigma_0)_{\lambda'\lambda} A(-\boldsymbol{\Delta}_\perp^2) + \frac{(\boldsymbol{\sigma}_{\lambda'\lambda} \times \mathrm{i}\boldsymbol{\Delta}_\perp)\cdot \hat{e}_z}{2m} B(-\boldsymbol{\Delta}_\perp^2) \right\} \\ & + m \frac{\bar{n}^{\{\mu} \big(\boldsymbol{\sigma}_{\lambda'\lambda} \times \mathrm{i}\boldsymbol{\Delta}_\perp \big)^{\nu\}}}{2m} J(-\boldsymbol{\Delta}_\perp^2) \\ & + m \left(\frac{\Delta_\perp^\mu \Delta_\perp^\nu + g^{\mu\nu}\boldsymbol{\Delta}_\perp^2}{4m^2} - \left(\frac{\boldsymbol{\Delta}_\perp^2}{4m^2} \right)^2 n^\mu n^\nu \right) \left((\sigma_0)_{\lambda'\lambda} - \frac{(\boldsymbol{\sigma}_{\lambda'\lambda} \times \mathrm{i}\boldsymbol{\Delta}_\perp)\cdot\hat{e}_z}{2m} \right) D(-\boldsymbol{\Delta}_\perp^2) \,. \end{aligned} \tag{64}$$

We remark immediately that Eq. (64) is independent of $\boldsymbol{P}$, as required for consistency of this approach. The result can thus be plugged into Eq. (43) to obtain the intrinsic, rest-frame EMT of a spin-half target.

As with the spin-zero target, we will use the dictionary in Eq. (17) to obtain energy and momentum densities and currents from the intrinsic EMT. We will find the nine Galilean components of the EMT—that is, the momentum densities and transverse stress tensor—reproduce results from standard light front coordinates, but the energy density, P_z fluxes, and longitudinal energy flux are newly-found by virtue of using tilted light front coordinates.

A. Momentum densities

We consider the momentum densities first. It is instructive to consider the P_z density and $\boldsymbol{P}_\perp$ densities in separate equations, as their behavior is quite different. From Eqs. (43) and (64), we find these densities to be:

$$\mathcal{P}_z(\boldsymbol{b}_\perp, \hat{\boldsymbol{s}}) = -t^0{}_3 = m \int \frac{\mathrm{d}^2\boldsymbol{\Delta}_\perp}{(2\pi)^2} \left(A(-\boldsymbol{\Delta}_\perp^2) + \frac{(\hat{\boldsymbol{s}} \times \mathrm{i}\boldsymbol{\Delta}_\perp)\cdot\hat{e}_z}{2m} B(-\boldsymbol{\Delta}_\perp^2) \right) \mathrm{e}^{-\mathrm{i}\boldsymbol{\Delta}_\perp\cdot\boldsymbol{b}_\perp} \tag{65a}$$

$$\boldsymbol{\mathcal{P}}_\perp(\boldsymbol{b}_\perp, \hat{\boldsymbol{s}}) = -t^0{}_1 \hat{e}_x - t^0{}_2 \hat{e}_y = m(\hat{\boldsymbol{s}}\cdot\hat{e}_z) \int \frac{\mathrm{d}^2\boldsymbol{\Delta}_\perp}{(2\pi)^2} \frac{\hat{e}_z \times \mathrm{i}\boldsymbol{\Delta}_\perp}{2m} J(-\boldsymbol{\Delta}_\perp^2)\, \mathrm{e}^{-\mathrm{i}\boldsymbol{\Delta}_\perp\cdot\boldsymbol{b}_\perp} \,. \tag{65b}$$

The P_z density reproduces prior results for the P^+ density in standard light front coordinates [68] if one sets $P^+ \to m$. For a free point fermion, $A(\Delta^2) = 1$ and $B(\Delta^2) = 0$, so the P_z density just becomes $m\delta^{(2)}(\boldsymbol{b}_\perp)$. This is expected because P_z is the central charge of the Galilean subgroup and is preserved by transverse boosts, so the barycentric coordinate $\boldsymbol{R}_\perp$ is a center-of-P_z coordinate and the intrinsic densities are relative to the center-of-P_z. (This has been explained in terms of standard light front coordinates by Lorcé [69].)

For non-pointlike targets with $B(\Delta^2) \neq 0$, transversely-polarized states will exhibit azimuthal modulations in the P_z density. The behavior is analogous to the modulations in its charge density [33], and is likewise induced by the synchronization scheme—specifically by modulations in the apparent clock rate of matter revolving around the target's center. It is worth pointing out that $F_2(\Delta^2)$—which controls the charge density modulations—and $B(\Delta^2)$ are Mellin moments of the same generalized parton distribution (GPD) $E(x, \xi, \Delta^2)$, suggesting that this GPD has an interpretation in terms of encoding partonic motion.

Despite the presence of these modulations, there is not a P_z dipole moment. This would of course contradict the barycenter being the center-of-P_z. If one calculates the P_z dipole moment from Eq. (65):

$$\langle \boldsymbol{b}_\perp \rangle_{p_z} = \int \mathrm{d}^2\boldsymbol{p}_\perp\, \boldsymbol{p}_\perp \mathcal{P}_z(\boldsymbol{b}_\perp, \hat{\boldsymbol{s}}) = \frac{\hat{e}_z \times \hat{\boldsymbol{s}}}{2m} B(0)\,. \tag{66}$$

However, $B(0) = 0$, a fact known as the vanishing of the anomalous gravitomagnetic moment [70]. It follows from the simultaneous sum rules $A(0) = 1$ (the momentum sum rule) and $J(0) = \frac{1}{2}$ (the angular momentum sum rule).

A radius can be associated with the P_z density:

$$\langle \boldsymbol{b}_\perp^2 \rangle_{p_z} = \int \mathrm{d}^2\boldsymbol{b}_\perp\, \mathcal{P}_z(\boldsymbol{b}_\perp, \hat{\boldsymbol{s}}) = 4\frac{\mathrm{d}A(\Delta^2)}{\mathrm{d}\Delta^2}\bigg|_{\Delta^2=0}\,. \tag{67}$$

This radius has appeared in the literature before. It has been called a P^+ radius in standard light front coordinates [17], and occasionally called a mass radius. (As pointed out by Lorcé *et al.* [8], mass plays several roles in relativity, and the P^+ radius could be considered a kind of mass radius. This is distinct, however, from the energy radius, which we give in Eq. (73).)

The $\boldsymbol{P}_\perp$ density in Eq. (65) would be the same in standard light front coordinates being a Galilean component of the EMT, but to the best of our knowledge this result has not been previously reported. This density is related to and tracks the z component of the *total* angular momentum density, the latter being

$$\mathcal{J}_z(\boldsymbol{b}_\perp, \hat{\boldsymbol{s}}) = \big(\boldsymbol{b}_\perp \times \boldsymbol{\mathcal{P}}_\perp(\boldsymbol{b}_\perp, \hat{\boldsymbol{s}})\big) \cdot \hat{e}_z\,. \tag{68}$$

This may appear counter-intuitive on first sight, as it superficially resembles the formula $\boldsymbol{r} \times \boldsymbol{p}$ for the *orbital* angular momentum of a body. However, the symmetric Belinfante EMT appears as the source of gravitation in general relativity, and the equivalence principle implies that all angular momentum should gravitate the same way. Thus, neither the Belinfante EMT nor its associated densities should be able to distinguish between spin and orbital angular momentum.

Moreover, despite the superficial resemblance, the right-hand side of Eq. (68) does not give an OAM density—at least not in terms of how OAM is usually defined. The amount of momentum $\boldsymbol{\mathcal{P}}_\perp(\boldsymbol{b}_\perp, \hat{\boldsymbol{s}})\,\mathrm{d}^2\boldsymbol{b}_\perp$ contained in a small spatial region $\mathrm{d}^2\boldsymbol{b}_\perp$ is not necessarily the momentum carried by a constituent of the target. This is especially clear if the target under consideration is a pointlike particle. The particle itself is an excitation of a field, which is the more fundamental object in quantum field theory. The momentum element $\boldsymbol{\mathcal{P}}_\perp(\boldsymbol{b}_\perp, \hat{\boldsymbol{s}})\,\mathrm{d}^2\boldsymbol{b}_\perp$ is the amount of momentum carried *by the field* in this small spatial region. However the only particle present is the target itself, which is at rest, so the OAM is zero. Thus Eq. (68) does not encode an OAM density.

B. Energy fluxes

From Eqs. (43) and (64), we find the energy fluxes to be:

$$\begin{aligned}\boldsymbol{\mathcal{F}}_E(\boldsymbol{b}_\perp, \hat{\boldsymbol{s}}) = t^i{}_0 \hat{e}_i = m \int \frac{\mathrm{d}^2\boldsymbol{\Delta}_\perp}{(2\pi)^2} \frac{\hat{\boldsymbol{s}} \times \mathrm{i}\boldsymbol{\Delta}_\perp}{2m} J(-\boldsymbol{\Delta}_\perp^2)\, \mathrm{e}^{-\,\mathrm{i}\boldsymbol{\Delta}_\perp \cdot \boldsymbol{b}_\perp} \\ + m\delta^{3i} \int \frac{\mathrm{d}^2\boldsymbol{\Delta}_\perp}{(2\pi)^2} \left[1 - \frac{(\hat{\boldsymbol{s}} \times \mathrm{i}\boldsymbol{\Delta}_\perp)\cdot \hat{e}_z}{2m}\right] \left(\frac{\boldsymbol{\Delta}_\perp^2}{4m^2}\right)^2 D(-\boldsymbol{\Delta}_\perp^2)\, \mathrm{e}^{-\,\mathrm{i}\boldsymbol{\Delta}_\perp \cdot \boldsymbol{b}_\perp}\,.\end{aligned} \tag{69}$$

We have separated the energy flux into two distinct pieces. The first of these involves a Fourier transform of the angular momentum form factor $J(\Delta^2)$. This term looks like an energy flux due to orbital motion, the transverse energy flux in particular being equal to the transverse momentum density. This mimics the well-known fact that the symmetric EMT in instant form coordinates has identical momentum densities and energy fluxes.

The second piece of Eq. (69) is a synchronization-induced energy flux in the z direction. It has the same origin and a similar form to the spin-zero energy flux of Eq. (51), but can contain additional azimuthal modulations when the target is transversely polarized.

C. Stress tensor and momentum fluxes

We next consider the intrinsic stress tensor of a spin-half target. From Eqs. (43) and (64),

$$\begin{aligned}S^{ij}(\boldsymbol{b}_\perp, \hat{\boldsymbol{s}}) \equiv -t^i{}_j(\boldsymbol{b}_\perp) = m\delta^{3j} \int \frac{\mathrm{d}^2\boldsymbol{\Delta}_\perp}{(2\pi)^2} \frac{(\hat{\boldsymbol{s}} \times \mathrm{i}\boldsymbol{\Delta}_\perp)^i}{2m} J(-\boldsymbol{\Delta}_\perp^2)\, \mathrm{e}^{-\,\mathrm{i}\boldsymbol{\Delta}_\perp \cdot \boldsymbol{b}_\perp} \\ + \frac{1}{4m} \int \frac{\mathrm{d}^2\boldsymbol{\Delta}_\perp}{(2\pi)^2} \left(\Delta_\perp^i \Delta_\perp^j - \delta^{ij}\boldsymbol{\Delta}_\perp^2\right) \left[1 - \frac{(\hat{\boldsymbol{s}} \times \mathrm{i}\boldsymbol{\Delta}_\perp)\cdot \hat{e}_z}{2m}\right] D(-\boldsymbol{\Delta}_\perp^2)\, \mathrm{e}^{-\,\mathrm{i}\boldsymbol{\Delta}_\perp \cdot \boldsymbol{b}_\perp}\,.\end{aligned} \tag{70}$$

Like with the energy fluxes, we have broken the result into two pieces, the first of which depends on the angular momentum form factor $J(\varDelta^2)$, and the other of which depends on the form factor $D(\varDelta^2)$.

The first angular momentum piece of the stress tensor is peculiar, in that it introduces asymmetric shear stresses. Recalling that the stress tensor consists of momentum fluxes, this piece of the stress tensor encodes fluxes of P_z in all three spatial directions, but not of $\boldsymbol{P}_\perp$. Now, a major difference between P_z and $\boldsymbol{P}_\perp$ in tilted coordinates is that the former is non-zero even if the velocity is zero; a P_z flux cannot be interpreted as a flux of some quantity of motion. Since classically $\boldsymbol{p}_\perp = p_z \boldsymbol{v}_\perp$ and $p_z - E = p_z v_z$, it should perhaps be the P_z flux minus the energy flux that is compared to the $\boldsymbol{P}_\perp$ flux:

$$\boldsymbol{\mathcal{F}}_{p_z}(\boldsymbol{b}_\perp, \hat{\boldsymbol{s}}) - \boldsymbol{\mathcal{F}}_E(\boldsymbol{b}_\perp, \hat{\boldsymbol{s}}) = -m\hat{e}_z \int \frac{\mathrm{d}^2\boldsymbol{\varDelta}_\perp}{(2\pi)^2} \frac{\boldsymbol{\varDelta}_\perp^2}{4m} \left(1 - \frac{\boldsymbol{\varDelta}_\perp^2}{4m}\right) \left[1 - \frac{(\hat{\boldsymbol{s}} \times \mathrm{i}\boldsymbol{\varDelta}_\perp)\cdot \hat{e}_z}{2m}\right] D(-\boldsymbol{\varDelta}_\perp^2)\, \mathrm{e}^{-\mathrm{i}\boldsymbol{\varDelta}_\perp \cdot \boldsymbol{b}_\perp} . \tag{71}$$

For comparison, the transverse components of the stress tensor are:

$$S_\perp^{ij}(\boldsymbol{b}_\perp, \hat{\boldsymbol{s}}) = \frac{1}{4m} \int \frac{\mathrm{d}^2\boldsymbol{\varDelta}_\perp}{(2\pi)^2} \left(\varDelta_\perp^i \varDelta_\perp^j - \delta_\perp^{ij} \boldsymbol{\varDelta}_\perp^2\right) \left[1 - \frac{(\hat{\boldsymbol{s}} \times \mathrm{i}\boldsymbol{\varDelta}_\perp)\cdot \hat{e}_z}{2m}\right] D(-\boldsymbol{\varDelta}_\perp^2)\, \mathrm{e}^{-\mathrm{i}\boldsymbol{\varDelta}_\perp \cdot \boldsymbol{b}_\perp} . \tag{72}$$

Both of these include only the form factor $D(\varDelta^2)$, which vanishes in the case of a pointlike particle [71] and can be interpreted as encoding internal dynamics in composite fermions [71]. For pointlike fermions, then, the energy and P_z fluxes are not zero, but are instead equal, and differences between them are an indication of dynamics and internal motion.

As a last remark, we note that the transverse P_z flux is equal to the $\boldsymbol{P}_\perp$ density, i.e., $\boldsymbol{\mathcal{F}}_{p_z}^{(\perp)}(\boldsymbol{b}_\perp, \hat{\boldsymbol{s}}) = \boldsymbol{\mathcal{P}}_\perp(\boldsymbol{b}_\perp, \hat{\boldsymbol{s}})$. This seems to comport with the classical tilted coordinate relation $\boldsymbol{p}_\perp = p_z \boldsymbol{v}_\perp$ if it is applied to the momentum carried by the target in any small region of space. Since this was a classical relation derived for observable bodies that obey the mass-shell relation $p^2 = m^2$, it is not a formal necessity that small elements of momenta supported by an infinitesimal region of space obey this relation.

D. Energy density

The last component of the intrinsic EMT to consider is the energy density. From Eqs. (43) and (64), using $\mathcal{E}(\boldsymbol{b}_\perp, \hat{\boldsymbol{s}}) = t^0{}_0(\boldsymbol{b}_\perp, \hat{\boldsymbol{s}})$ gives exactly Eq. (2) given in the introduction. The spin-independent piece of the spin-half energy density is identical to the spin-zero energy density of Eq. (46). The spin-dependent piece does not contribute to the energy radius, which is therefore identical to the spin-zero case:

$$\langle \boldsymbol{b}_\perp^2 \rangle_{\text{energy}} \equiv \frac{1}{m} \int \mathrm{d}^2\boldsymbol{b}_\perp\, \boldsymbol{b}_\perp^2\, \mathcal{E}(\boldsymbol{b}_\perp, \hat{\boldsymbol{s}}) = 4 \frac{\mathrm{d}A(\varDelta^2)}{\mathrm{d}\varDelta^2}\bigg|_{\varDelta^2=0} - \frac{1}{m^2} D(0) . \tag{73}$$

The spin-dependent part of the EMT introduces angular modulations through several of the form factors, which must be attributed to distinct physical effects. The angular modulations introduced through the form factor $B(\varDelta^2)$ can be attributed to clock rate modulations, as explained for the P_z density in Sec. V A. In particular, modulations due to $B(\varDelta^2)$ will increase density on the side of the hadron moving away from the observer.

The angular momentum form factor $J(\varDelta^2)$ contributes to angular modulations with the opposite sign from $B(\varDelta^2)$, thus causing the density to increase on the side moving towards the observer. This is effectively an artifact of the density being defined with respect to the center-of-P_z. Since $B(0) = 0$, the amount of P_z on each side of the spin axis in a transversely-polarized fermion is the same. If the classical relation $p_z - E = p_z v_z$ is assumed to hold for each half of the fermion, the half moving towards the observer has $v_z < 0$ and thus should have greater energy, and the half moving away should have less energy. The modulations in the energy density arising from $J(\varDelta^2)$ accomplish just this. In fact, by comparing Eqs. (65), (70) and (2) we find:

$$\mathcal{P}_z(\boldsymbol{b}_\perp, \hat{\boldsymbol{s}}) - \mathcal{E}(\boldsymbol{b}_\perp, \hat{\boldsymbol{s}}) = \hat{e}_z \cdot \boldsymbol{\mathcal{F}}_{p_z}(\boldsymbol{b}_\perp, \hat{\boldsymbol{s}}) , \tag{74}$$

meaning that $p_z - E = p_z v_z$ apparently holds for infinitesimal elements of the hadron everywhere on the transverse plane.

In contrast to the P_z density, the energy density entails a synchronization-induced energy dipole moment:

$$\boldsymbol{d}_E \equiv \langle \boldsymbol{b}_\perp \rangle_E = \int \mathrm{d}^2\boldsymbol{b}_\perp\, \boldsymbol{b}_\perp \mathcal{E}(\boldsymbol{b}_\perp, \hat{\boldsymbol{s}}) = -\frac{\hat{e}_z \times \hat{\boldsymbol{s}}}{2} J(0) = -\frac{1}{4} \hat{e}_z \times \hat{\boldsymbol{s}} . \tag{75}$$

We reiterate and stress that this apparent dipole moment arises from the proton's "center" being given by the center-of-P_z rather than the center-of-energy. However, the remaining modulations from the form factors $B(t)$ and $D(t)$—which do not contribute to the dipole moment—may be due to clock rate modulations, similar to the modulations in the P_z density.

E. Numerical estimates for the proton

We now consider what the energy and momentum densities and currents might look like for the proton. Currently, high-precision empirical results for the proton's gravitational form factors do not exist. There are model-dependent estimates, which we shall utilize in building simple parametrizations for the form factors. However, the results shown here should be taken as just illustrative of the formalism because of the lack of precision data.

The quark contribution to $D(t)$ has been estimated by Burkert *et al.* [72, 73] using a dispersive analysis of DVCS data from CLAS at Jefferson Lab. The extraction depends on assumptions about the functional form of the Compton form factors, as explained in a response by Kumericki [74]. This leads to unquantified systematic uncertainties in the dispersive analysis, though we will utilize their parameters in building a parametrization for the sake of illustration. Burkert *et al.* assume a tripole form for $D(t)$ in their first analysis [72] and a multipole form with a floating power in their second [73], though the result of the latter are compatible with a tripole within uncertainty.

Additionally, the gluon contributions to the form factors $A(t)$ and $D(t)$ have been estimated by Duran *et al.* [75] using near-threshold J/ψ production from a proton target as part of the J/ψ-007 experiment (E12-16-007) in Hall C at Jefferson Lab. In the original report of Duran *et al.*, there is a discrepancy between the form factors when a holographic model and when a GPD-based model is used in the extraction. However, Guo *et al.* [76] report that the original formulation of the GPD-based model contained a factor 2 error, and that the discrepancy is reduced significantly upon correcting for this.

Nonetheless, the extractions of Duran *et al.* were obtained by assuming a tripole form for both $A(t)$ and $D(t)$. Quark counting rules suggest that $D(t) \sim (-t)^{-3}$ at large $-t$—indeed compatible with the tripole form—but that $A(t) \sim (-t)^{-2}$ instead; see Masjuan *et al.* [77] for instance.

In light of these concerns, we resort to the following simplified forms for the gravitational form factors:

$$A(-\boldsymbol{\Delta}_\perp^2) = 2J(-\boldsymbol{\Delta}_\perp^2) = \frac{1}{(1+\boldsymbol{\Delta}_\perp^2/m_{A1}^2)(1+\boldsymbol{\Delta}_\perp^2/m_{A2}^2)} \tag{76a}$$

$$D(-\boldsymbol{\Delta}_\perp^2) = \frac{d_0}{(1+\boldsymbol{\Delta}_\perp^2/m_{D1}^2)(1+\boldsymbol{\Delta}_\perp^2/m_{D2}^2)(1+\boldsymbol{\Delta}_\perp^2/m_{D3}^2)} \tag{76b}$$

$$B(-\boldsymbol{\Delta}_\perp^2) = 0\,. \tag{76c}$$

These forms for A and D are inspired by the work of Masjuan *et al.* [77]. They both account for the expected large $-t$ falloff and the presence of poles from meson dominance. In particular, $A(t)$ has only spin-two meson poles and $D(t)$ can have both spin-zero and spin-two poles. At zero and spacelike t, the form factors should be dominated by the lightest meson poles. We use the central values of the Breit-Wigner masses from the Particle Data Group [78] for these:

$$m_{D1} = m(f_0(500)) = 600 \pm 200 \text{ MeV} \tag{77a}$$

$$m_{D2} = m(f_0(980)) = 990 \pm 20 \text{ MeV} \tag{77b}$$

$$m_{A1} = m_{D3} = m(f_2(1270)) = 1275.4 \pm 0.8 \text{ MeV} \tag{77c}$$

$$m_{A2} = m(f_2'(1525)) = 1517.4 \pm 2.5 \text{ MeV} \tag{77d}$$

We use $B(t) = 0$ because lattice calculations [79, 80] suggest that this form factor is small.

Lastly, for d_0, we add the quark estimate from Burkert *et al.* of $-1.47 \pm 0.06 \pm 0.14$ with the gluon estimate from Duran *et al.* (via the holographic model) of -1.8 ± 0.528 to get

$$d_0 = -3.27 \pm 0.55\,, \tag{78}$$

where we added the reported errors in quadrature.

We now proceed to obtain the EMT densities of the proton. Because we are using $B(t) = 0$, the P_z density is independent of polarization. From Eq. (65) and Eq. (76), the P_z density is:

$$\mathcal{P}_z(\boldsymbol{b}_\perp, \hat{\boldsymbol{s}}) = \frac{1}{2\pi}\frac{m_{A1}^2 m_{A2}^2}{m_{A2}^2 - m_{A1}^2}\Big(K_0(m_{A1}b_\perp) - K_0(m_{A2}b_\perp)\Big) \tag{79}$$

where $K_\nu(x)$ is a modified Bessel function of the second kind [81]. It's worth noting that this density is finite at the origin:

$$\lim_{b_\perp\to 0}\mathcal{P}_z(\boldsymbol{b}_\perp, \hat{\boldsymbol{s}}) = \frac{1}{2\pi}\frac{m_{A1}^2 m_{A2}^2}{m_{A2}^2 - m_{A1}^2}\log\left(\frac{m_{A2}}{m_{A1}}\right)\,, \tag{80}$$

in contrast to the 2D Fourier transform of a monopole form [82]. Similarly obtainable from Eqs. (65) and (76) is the transverse momentum density:

$$\boldsymbol{\mathcal{P}}_\perp(\boldsymbol{b}_\perp, \hat{\boldsymbol{s}}) = \frac{(\hat{\boldsymbol{s}}\cdot\hat{e}_z)(\hat{e}_y\cos\phi - \hat{e}_x\sin\phi)}{8\pi}\frac{m_{A1}^2 m_{A2}^2}{m_{A2}^2 - m_{A1}^2}\Big(m_{A1}K_1(m_{A1}b_\perp) - m_{A2}K_1(m_{A2}b_\perp)\Big)\,, \tag{81}$$

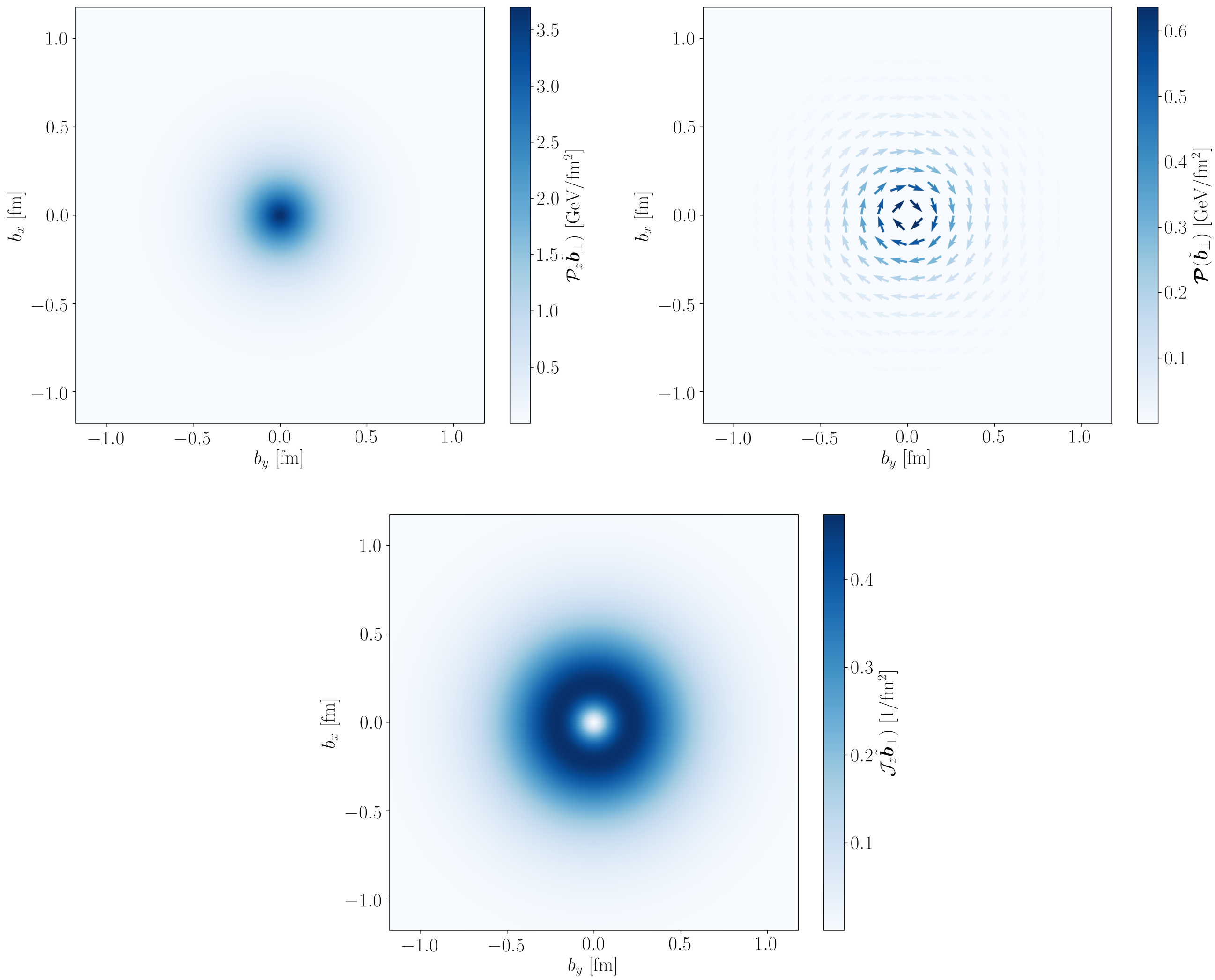

FIG. 3. Momentum and angular momentum densities in a proton. (Left panel) is the P_z density, which is independent of polarization under the assumption $B(t) = 0$. (Middle panel) is the $\boldsymbol{P}_\perp$ density in a proton that is spin-up along the z-axis. (Right panel) is the J_z (angular momentum) density in a proton that is spin-up along the z-axis. In these plots, the x-axis is oriented vertically and the y-axis horizontally so that the z axis points into the page, allowing plots to mimic what an observer would see at fixed light front time.

from which it follows that the density of the z component of angular momentum is:

$$\mathcal{J}_z(\boldsymbol{b}_\perp, \hat{\boldsymbol{s}}) = \frac{(\hat{\boldsymbol{s}} \cdot \hat{e}_z) b_\perp}{8\pi} \frac{m_{A1}^2 m_{A2}^2}{m_{A2}^2 - m_{A1}^2} \Big(m_{A1} K_1(m_{A1} b_\perp) - m_{A2} K_1(m_{A2} b_\perp) \Big) . \tag{82}$$

Numerical results for the momentum and angular momentum densities for a longitudinally-polarized proton are presented in Fig. 3. The P_z density is unchanged for transversely-polarized protons owing to the assumption $B(t) = 0$, while the $\boldsymbol{P}_\perp$ and J_z densities vanish identically for transversely-polarized protons. The angular momentum density has an apparent hole in it because of the factor $b_\perp$, which reduces it near the origin.

The energy and momentum flux densities are our next consideration. The transverse components of the stress tensor have previously been considered in Refs. [16, 17, 47, 83], with Ref. [47] in particular exploring the distortions in eigenpressure directions that occur in transversely-polarized states. Since tilted coordinates newly allow access to energy and P_z flux densities, we will focus on these specifically.

As explained in Sec. V C, the transverse P_z flux is equal to the $\boldsymbol{P}_\perp$ density; and as pointed out in Sec. V B, it is also equal to the transverse energy flux due to symmetry of the EMT. Thus:

$$\boldsymbol{\mathcal{F}}_E^{(\perp)}(\boldsymbol{b}_\perp, \hat{\boldsymbol{s}}) = \boldsymbol{\mathcal{F}}_{p_z}^{(\perp)}(\boldsymbol{b}_\perp, \hat{\boldsymbol{s}}) = \frac{(\hat{\boldsymbol{s}} \cdot \hat{e}_z)(\hat{e}_y \cos\phi - \hat{e}_x \sin\phi)}{8\pi} \frac{m_{A1}^2 m_{A2}^2}{m_{A2}^2 - m_{A1}^2} \Big(m_{A1} K_1(m_{A1} b_\perp) - m_{A2} K_1(m_{A2} b_\perp) \Big) . \tag{83}$$

Since these are exactly equal to the $\boldsymbol{P}_\perp$ density, we point the reader to the middle panel of Fig. 3 for an estimate of these quantities for a longitudinally-polarized proton.

The longitudinal P_z flux, which can also be interpreted as pressure in the z direction (since it is a normal stress) can be obtained by putting Eq. (76) into Eq. (70) with $i = j = 3$. The expressions involving Fourier transforms of $D(t)$ can get complicated. To reduce their lengths, it is helpful to define coefficients:

$$c_1 = \frac{m_{D2}^2 m_{D3}^2 (m_{D2}^2 - m_{D3}^2)}{m_{D1}^2 m_{D2}^2 (m_{D1}^2 - m_{D2}^2) + m_{D2}^2 m_{D3}^2 (m_{D2}^2 - m_{D3}^2) + m_{D3}^2 m_{D1}^2 (m_{D3}^2 - m_{D1}^2)} \tag{84a}$$

$$c_2 = \frac{m_{D3}^2 m_{D1}^2 (m_{D3}^2 - m_{D1}^2)}{m_{D1}^2 m_{D2}^2 (m_{D1}^2 - m_{D2}^2) + m_{D2}^2 m_{D3}^2 (m_{D2}^2 - m_{D3}^2) + m_{D3}^2 m_{D1}^2 (m_{D3}^2 - m_{D1}^2)} \tag{84b}$$

$$c_3 = \frac{m_{D1}^2 m_{D2}^2 (m_{D1}^2 - m_{D2}^2)}{m_{D1}^2 m_{D2}^2 (m_{D1}^2 - m_{D2}^2) + m_{D2}^2 m_{D3}^2 (m_{D2}^2 - m_{D3}^2) + m_{D3}^2 m_{D1}^2 (m_{D3}^2 - m_{D1}^2)} , \tag{84c}$$

which are obtained through a partial fraction decomposition:

$$\frac{1}{(1 + \boldsymbol{\Delta}_\perp^2 / m_{D1}^2)(1 + \boldsymbol{\Delta}_\perp^2 / m_{D2}^2)(1 + \boldsymbol{\Delta}_\perp^2 / m_{D3}^2)} = \sum_{n=1}^{3} \frac{c_n}{1 + \boldsymbol{\Delta}_\perp^2 / m_{Dn}^2} , \tag{84d}$$

and which accordingly have the following properties:

$$c_1 + c_2 + c_3 = 1 \tag{84e}$$

$$m_{D1}^2 c_1 + m_{D2}^2 c_2 + m_{D3}^2 c_3 = 0 \tag{84f}$$

$$m_{D1}^4 c_1 + m_{D2}^4 c_2 + m_{D3}^4 c_3 = 0 . \tag{84g}$$

The resulting expression for the longitudinal pressure is then:

$$\begin{aligned} p_z(\boldsymbol{b}_\perp, \hat{\boldsymbol{s}}) = \mathcal{F}_{p_z}^{(z)}(\boldsymbol{b}_\perp, \hat{\boldsymbol{s}}) &= \frac{\hat{b}_\perp \cdot (\hat{e}_z \times \hat{\boldsymbol{s}})}{8\pi} \frac{m_{A1}^2 m_{A2}^2}{m_{A2}^2 - m_{A1}^2} \Big(m_{A1} K_1(m_{A1} b_\perp) - m_{A2} K_1(m_{A2} b_\perp) \Big) \\ &+ d_0 \sum_{n=1}^{3} c_n \frac{m_{Dn}^4}{4\pi m} \left(K_0(m_{Dn} b_\perp) + \hat{b}_\perp \cdot (\hat{e}_z \times \hat{\boldsymbol{s}}) \frac{m_{Dn}}{2m} K_1(m_{Dn} b_\perp) \right) . \end{aligned} \tag{85}$$

We can similarly obtain the longitudinal energy flux by plugging Eq. (76) into Eq. (69) with $i = 3$. The result is:

$$\begin{aligned} \mathcal{F}_E^{(z)}(\boldsymbol{b}_\perp, \hat{\boldsymbol{s}}) &= \frac{\hat{b}_\perp \cdot (\hat{e}_z \times \hat{\boldsymbol{s}})}{8\pi} \frac{m_{A1}^2 m_{A2}^2}{m_{A2}^2 - m_{A1}^2} \Big(m_{A1} K_1(m_{A1} b_\perp) - m_{A2} K_1(m_{A2} b_\perp) \Big) \\ &+ d_0 \sum_{n=1}^{3} c_n \frac{m_{Dn}^6}{32\pi m^3} \left(K_0(m_{Dn} b_\perp) + \hat{b}_\perp \cdot (\hat{e}_z \times \hat{\boldsymbol{s}}) \frac{m_{Dn}}{2m} K_1(m_{Dn} b_\perp) \right) . \end{aligned} \tag{86}$$

From Eq. (84g) it follows that the longitudinal pressure is finite at the origin:

$$\lim_{b_\perp \to 0} p_z(\boldsymbol{b}_\perp, \hat{\boldsymbol{s}}) = -d_0 \lim_{b_\perp \to 0} \sum_{n=1}^{3} c_n \frac{m_{Dn}^4}{4\pi m} \log(m_{Dn} b_\perp) = d_0 \sum_{n=1}^{3} c_n \frac{m_{Dn}^4}{4\pi m} \log\left(\frac{m}{m_{Dn}} \right) . \tag{87}$$

By contrast, the longitudinal energy flux is not finite. On the one hand, this can be seen as occurring because there is no rule analogous to Eq. (84g) for sixth powers of the meson pole masses. This can also be seen by considering that in momentum space, the quantity $\boldsymbol{\Delta}_\perp^4 D(-\boldsymbol{\Delta}_\perp^2)$ goes as $\boldsymbol{\Delta}_\perp^{-2}$ at very large $|\boldsymbol{\Delta}_\perp|$, and accordingly its contribution to the integral in Eq. (69) will diverge logarithmically when $\boldsymbol{b}_\perp = 0$.

Numerical results for longitudinal P_z and energy fluxes are presented for longitudinally and transversely polarized protons in Fig. 4. Because of the singularity of the energy flux at the origin, the maximum value of the energy flux has been clipped. These flux densities all integrate to zero, which may be difficult to see by eye in these plots; for instance, the core of negative energy flux

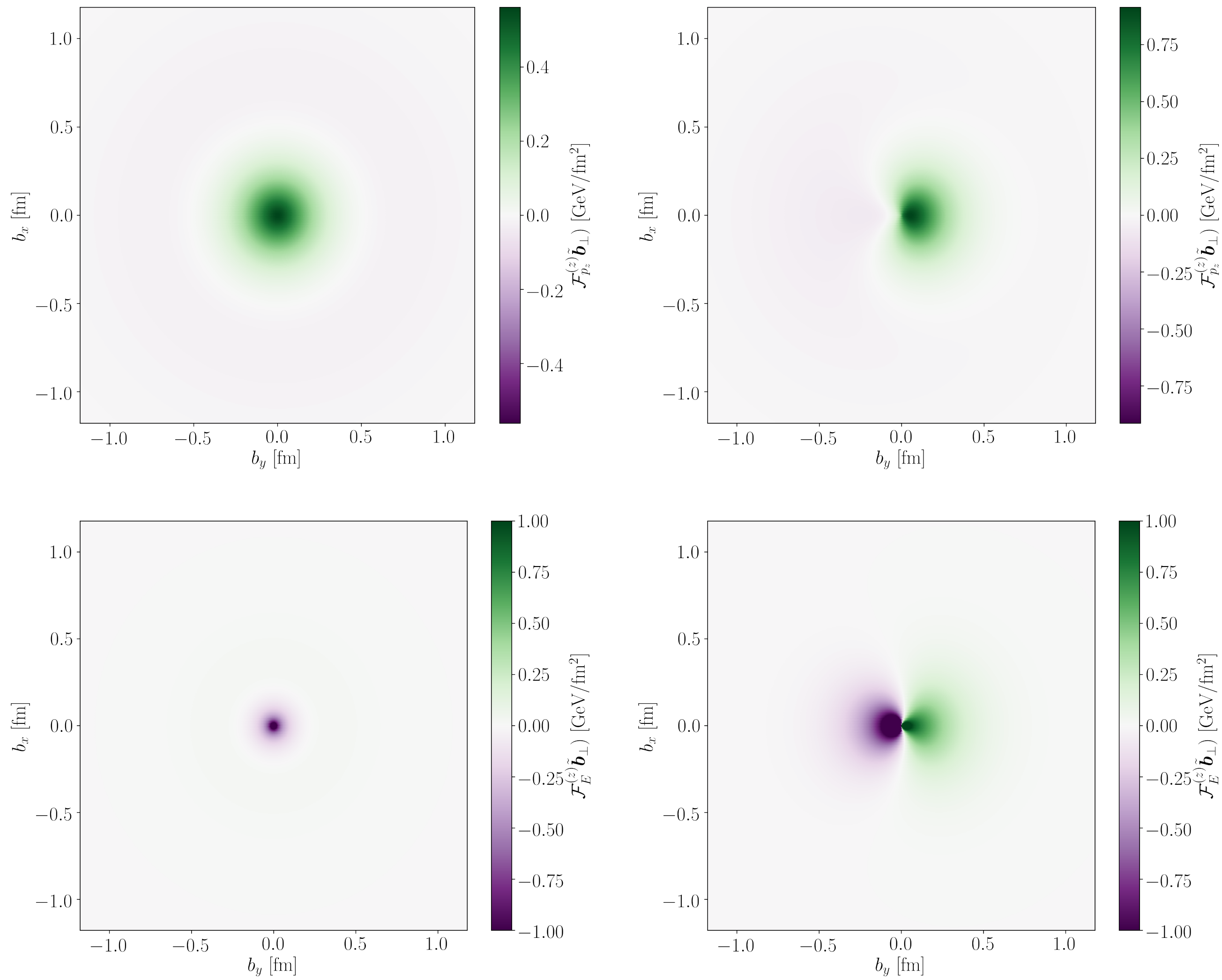

FIG. 4. P_z flux density (top row) and energy flux density (bottom row) in the z direction, both for protons polarized with spin up along the z axis (left column) and spin up along the x axis (right column). For the energy flux plots, the largest magnitudes mapped are clipped at 1 GeV/fm^2; since the energy flux density is singular at the origin, there would be no maximum without clipping. In these plots, the x-axis is oriented vertically and the y-axis horizontally so that the z axis points into the page, allowing plots to mimic what an observer would see at fixed light front time. Accordingly, positive flux is into the page (away from the observer) and negative flux is out of the page (towards the observer).

in the lower-left panel is surrounded by a diffuse cloud of positive energy flux. One-dimensional reductions of the flux densities for longitudinally polarized protons are presented later, in Fig. 6, where the vanishing of the net flux may be easier to see.

Finally, from Eqs. (2) and (76) we obtain the energy density. It is perhaps simpler to decompose the energy density into a spin-dependent piece and a spin-independent piece as follows:

$$\mathcal{E}(\boldsymbol{b}_\perp, \hat{\boldsymbol{s}}) = \mathcal{E}(b_\perp) + \hat{b}_\perp \cdot (\hat{e}_z \times \hat{\boldsymbol{s}})\mathcal{E}_1(b_\perp)\,. \tag{88}$$

These pieces are respectively given in the simple multipole model by:

$$\mathcal{E}_0(b_\perp) = \mathcal{P}_z(b_\perp) - d_0 \sum_{n=1}^{3} c_n \frac{m_{Dn}^4}{4\pi m} K_0(m_{Dn} b_\perp) \tag{89a}$$

$$\mathcal{E}_1(b_\perp) = -|\boldsymbol{\mathcal{P}}_\perp(b_\perp)| - d_0 \sum_{n=1}^{3} c_n \frac{m_{Dn}^5}{8\pi m^2} K_1(m_{Dn} b_\perp)\,. \tag{89b}$$

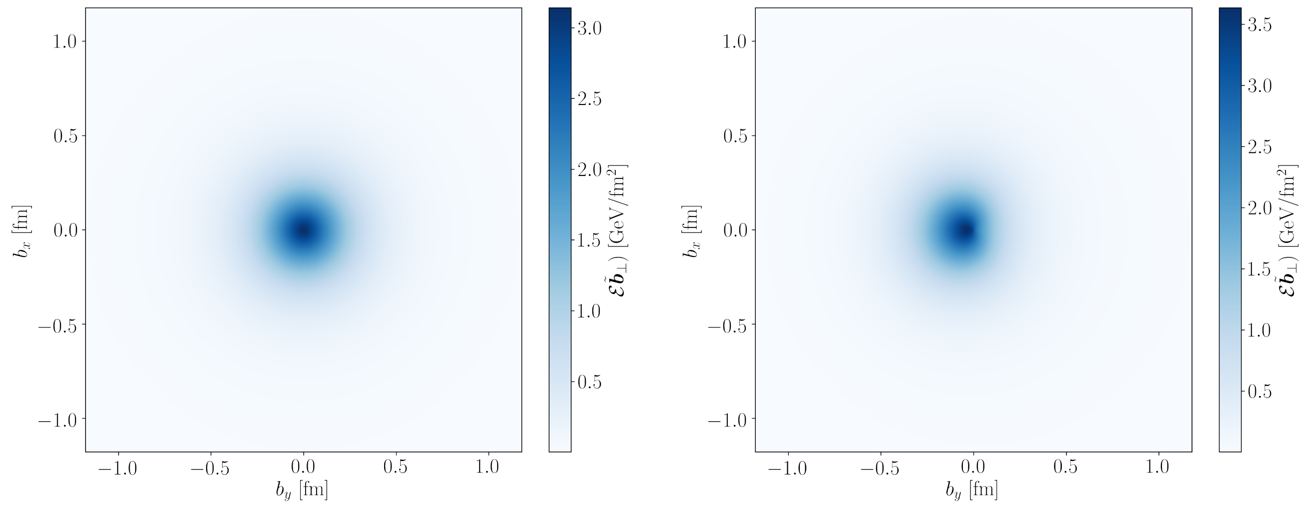

FIG. 5. Energy density for protons polarized with spin up along the z axis (left panel) and spin up along the x axis (right panel). In these plots, the x-axis is oriented vertically and the y-axis horizontally so that the z axis points into the page, allowing plots to mimic what an observer would see at fixed light front time.

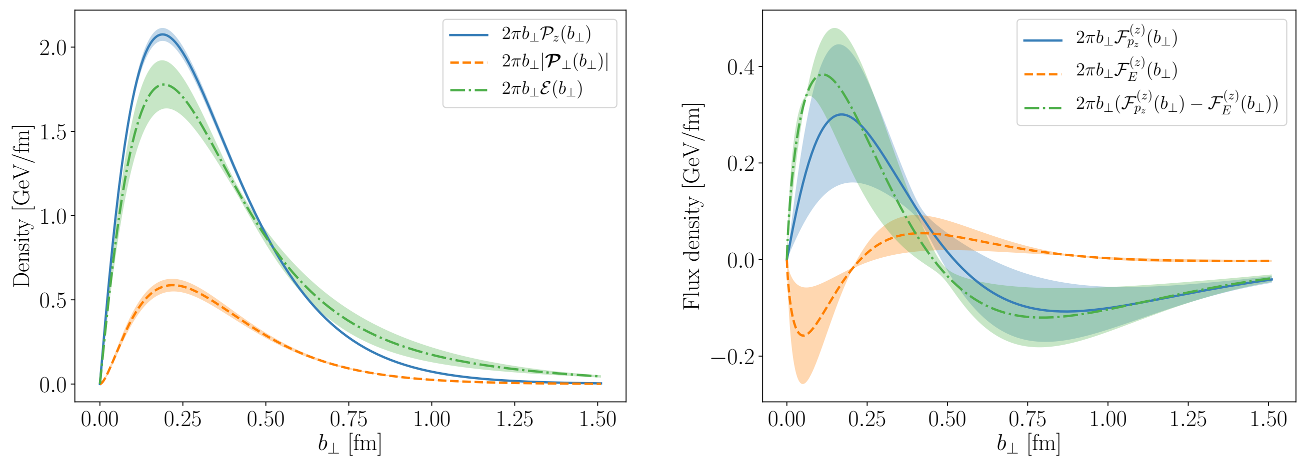

FIG. 6. One-dimensional reductions of the transverse momentum and energy densities (left panel) and flux densities (right panel) of a proton polarized along the z axis. The uncertainty bands incorporate only uncertainties in the multipole parameters as given in Eqs. (77) and (78).

Numerical results for the energy density are presented in Fig. 5. The right panel in particular shows the energy density of a transversely-polarized proton with its spin up along the x-axis. In these plots, the x-axis is vertical and the y-axis horizontal, so that the z-axis points into the page by the right-hand rule. This is done so that the plots are representative of what an observer would actually see at fixed light front time. The energy is lopsided on the side of the proton that is revolving towards the observer, in contrast to the modulations previously seen in the proton's charge density [33]. As explained in Sec. V D, these modulations have a different cause than the charge density modulations, which were the result of clock rate modulations. The energy density modulations are largely an artifact of the proton's center in the light front formalism being the center-of-P_z: there are equal amounts of P_z on both sides of the proton, and given the tilted coordinate relation $p_z v_z = p_z - E$, there must be more energy on the side with $v_z < 0$—i.e., the side moving towards the observer.

It is also instructive to consider one-dimensional reductions of the densities and currents we have calculated. Such reductions are presented in Fig. 6, specifically for the case of a longitudinally-polarized proton. Uncertainty bands have been included in these plots from propagating the uncertainties in the meson pole masses and in d_0. Notably, the uncertainty bands in the flux densities are quite large.

The left panel of Fig. 6 illustrates several interesting qualitative features of the energy and momentum densities. First of all, the magnitude of the transverse momentum density is much smaller than the P_z or energy densities. The P_z density, it should be recalled, is not a measure of motion in tilted coordinates, but can better be interpreted as a measure of inertia, and in fact the P_z density here integrates to the mass. It is thus not surprising that the P_z density is much larger than the $\boldsymbol{P}_\perp$ density. On the contrary, the $\boldsymbol{P}_\perp$ density is quite large, becoming as large as hundreds of MeV/fm, which is indicative of ultrarelativistic motion within the proton.

The left panel of Fig. 6 also qualitatively illustrates that the energy distribution in the proton is broader than the P_z distribution. Accordingly, the energy radius should be larger than the momentum radius. Given the values in Eqs. (77) and (78), as well as Eqs. (67) and (73) for the radii, we find:

$$\langle \boldsymbol{b}_\perp^2 \rangle_{P_z} = \frac{4}{m_{A1}^2} + \frac{4}{m_{A2}^2} = \big(0.40\ \mathrm{fm}\big)^2 \tag{90a}$$

$$\langle \boldsymbol{b}_\perp^2 \rangle_{E} = \frac{4}{m_{A1}^2} + \frac{4}{m_{A2}^2} - \frac{d_0}{m^2} = \big(0.55 \pm 0.02\ \mathrm{fm}\big)^2 . \tag{90b}$$

The uncertainty in the P_z radius propagated from uncertainties in the $f_2(1270)$ and $f_2'(1525)$ masses is smaller than the precision to which we quote the P_z radius. To be sure, these results all come from assuming a particular functional from for the gravitational form factors, and there is an unquantifiable amount of uncertainty associated with this choice. Future experiments aimed at extracting generalized parton distributions, such as deeply virtual Compton scattering [22–24, 84] and single-diffractive hard exclusive reactions [85], must be carried out to provide both more realistic estimates of the proton's gravitational form factors and more realistic uncertainty quantification.

F. Changes when using the asymmetric EMT

Before concluding, let us consider how the densities we have present would be modified by including an antisymmetric piece in the EMT, as defined in Eq. (8). This would introduce an additional form factor

$$\langle \boldsymbol{p}', \lambda' | \hat{T}_{\mathrm{A}}^{\mu\nu}(0) | \boldsymbol{p}, \lambda \rangle = \bar{u}(\boldsymbol{p}', \lambda') \gamma^{[\mu} P^{\nu]} u(\boldsymbol{p}, \lambda) S(\Delta^2) \tag{91}$$

which must be added to the breakdown in Eq. (61). Using formulas from Appendix A of Ref. [33], we can explicitly evaluate matrix elements of this when $\Delta_z = 0$ to be:

$$\langle \boldsymbol{p}', \lambda' | \hat{T}_{\mathrm{A}}^{\mu\nu}(0) | \boldsymbol{p}, \lambda \rangle = -\left\{ -\frac{\mathrm{i} P^{[\mu} \epsilon^{\nu]\rho\sigma\tau} n_\rho P_\sigma \Delta_\tau}{(P\cdot n)} (\sigma_3)_{\lambda'\lambda} + \frac{m P^{[\mu} n^{\nu]}}{(P\cdot n)} \mathrm{i} \epsilon^{\alpha\beta\gamma\delta} n_\alpha \bar{n}_\beta \Delta_\gamma (\sigma_\delta)_{\lambda'\lambda} \right\} S(-\boldsymbol{\Delta}_\perp^2) . \tag{92}$$

To obtain the rest frame quantity that we take a Fourier transform of, we must apply the inverse of the average-boost matrix $\bar{\Lambda}$. Using the formulas from Appendix B, we find:

$$(\bar{\Lambda}^{-1})^\mu{}_\alpha (\bar{\Lambda}^{-1})^\nu{}_\beta \frac{\langle \boldsymbol{p}', \lambda' | \hat{T}_{\mathrm{A}}^{\alpha\beta}(0) | \boldsymbol{p}, \lambda \rangle}{2m} = -m \frac{\bar{n}^{[\mu} \big(\boldsymbol{\sigma}_{\lambda'\lambda} \times \mathrm{i}\boldsymbol{\Delta}_\perp\big)^{\nu]}}{2m} S(-\boldsymbol{\Delta}_\perp^2) . \tag{93}$$

Adding the Fourier transform of this quantity to the previously obtained EMT densities would modify them in manners we shall presently explore.

Firstly, in the expression for the transverse momentum density $\boldsymbol{\mathcal{P}}_\perp(\boldsymbol{b}_\perp, \hat{\boldsymbol{s}})$ in Eq. (65), the form factor $J(-\boldsymbol{\Delta}_\perp^2)$ would be replaced by $J(-\boldsymbol{\Delta}_\perp^2) - S(-\boldsymbol{\Delta}_\perp^2)$, giving:

$$\boldsymbol{\mathcal{P}}_\perp^{(\mathrm{asym})}(\boldsymbol{b}_\perp, \hat{\boldsymbol{b}}_\perp) = \boldsymbol{\mathcal{P}}_\perp(\boldsymbol{b}_\perp, \hat{\boldsymbol{b}}_\perp) - m(\hat{e}_z \cdot \hat{\boldsymbol{s}}) \int \frac{\mathrm{d}^2\boldsymbol{\Delta}_\perp}{(2\pi)^2} \frac{\hat{e}_z \times \mathrm{i}\boldsymbol{\Delta}_\perp}{2m} S(-\boldsymbol{\Delta}_\perp^2)\, \mathrm{e}^{-\mathrm{i}\boldsymbol{\Delta}_\perp\cdot\boldsymbol{b}_\perp} . \tag{94}$$

Under the interpretation that $S(-\boldsymbol{\Delta}_\perp^2)$ encodes the spatial distribution of *fermion* spin, the $J - S$ difference encodes a combination of quark OAM and gluon total angular momentum. Accordingly, when using the asymmetric EMT, the transverse momentum density tracks this particular mix of contributions to the angular momentum. If no gluons were present in the hadron, $J(-\boldsymbol{\Delta}_\perp^2) - S(-\boldsymbol{\Delta}_\perp^2)$ would simply track OAM. It is interesting to note that for a free fermion, this form factor difference is zero, and the transverse momentum density in a free fermion thus vanishes for the asymmetric EMT.

Secondly, in the energy flux density $\boldsymbol{\mathcal{F}}_E(\boldsymbol{b}_\perp, \hat{\boldsymbol{s}})$ of Eq. (69), $J(-\boldsymbol{\Delta}_\perp^2)$ would be replaced by $J(-\boldsymbol{\Delta}_\perp^2) + S(-\boldsymbol{\Delta}_\perp^2)$, giving:

$$\boldsymbol{\mathcal{F}}_E^{(\mathrm{asym})}(\boldsymbol{b}_\perp, \hat{\boldsymbol{b}}_\perp) = \boldsymbol{\mathcal{F}}_E(\boldsymbol{b}_\perp, \hat{\boldsymbol{b}}_\perp) + m \int \frac{\mathrm{d}^2\boldsymbol{\Delta}_\perp}{(2\pi)^2} \frac{\hat{\boldsymbol{s}} \times \mathrm{i}\boldsymbol{\Delta}_\perp}{2m} S(-\boldsymbol{\Delta}_\perp^2)\, \mathrm{e}^{-\mathrm{i}\boldsymbol{\Delta}_\perp\cdot\boldsymbol{b}_\perp} . \tag{95}$$

Along the same vein, the e P_z flux is also modified by replacing $J(-\boldsymbol{\Delta}_\perp^2)$ with $J(-\boldsymbol{\Delta}_\perp^2) + S(-\boldsymbol{\Delta}_\perp^2)$ in Eq. (70) giving:

$$\mathcal{F}_{p_z}^{(\text{asym})}(\boldsymbol{b}_\perp, \hat{\boldsymbol{b}}_\perp) = \mathcal{F}_{p_z}(\boldsymbol{b}_\perp, \hat{\boldsymbol{b}}_\perp) + m(\hat{e}_z \cdot \hat{\boldsymbol{s}}) \int \frac{\mathrm{d}^2\boldsymbol{\Delta}_\perp}{(2\pi)^2} \frac{\hat{e}_z \times \mathrm{i}\boldsymbol{\Delta}_\perp}{2m} S(-\boldsymbol{\Delta}_\perp^2)\, \mathrm{e}^{-\mathrm{i}\boldsymbol{\Delta}_\perp \cdot \boldsymbol{b}_\perp} . \tag{96}$$

Notably, the transverse P_z flux and transverse momentum densities are no longer equal for the asymmetric EMT, meaning small elements of matter inside the hadron no longer obey the relation $\boldsymbol{p}_\perp = p_z \boldsymbol{v}_\perp$. Of course, there is no formal constraint that formal elements of matter (as opposed to on-shell particles) must obey this relation, so the asymmetric EMT is not inconsistent for this.

Lastly, the energy density $\mathcal{E}(\boldsymbol{b}_\perp, \hat{\boldsymbol{s}})$ is modified in Eq. (2) by replacing $J(-\boldsymbol{\Delta}_\perp^2)$ with $J(-\boldsymbol{\Delta}_\perp^2) - S(-\boldsymbol{\Delta}_\perp^2)$, giving:

$$\mathcal{E}^{(\text{asym})}(\boldsymbol{b}_\perp, \hat{\boldsymbol{b}}_\perp) = \mathcal{E}(\boldsymbol{b}_\perp, \hat{\boldsymbol{b}}_\perp) - m \int \frac{\mathrm{d}^2\boldsymbol{\Delta}_\perp}{(2\pi)^2} \frac{\hat{e}_z \cdot (\hat{\boldsymbol{s}} \times \mathrm{i}\boldsymbol{\Delta}_\perp)}{2m} S(-\boldsymbol{\Delta}_\perp^2)\, \mathrm{e}^{-\mathrm{i}\boldsymbol{\Delta}_\perp \cdot \boldsymbol{b}_\perp} . \tag{97}$$

It is interesting to note that for a free elementary fermion, $\mathcal{E}^{(\text{asym})}(\boldsymbol{b}_\perp, \hat{\boldsymbol{b}}_\perp) = m\delta^{(2)}(\boldsymbol{b}_\perp)$ regardless of polarization; since $J_{\text{free}}(-\boldsymbol{\Delta}_\perp^2) = S_{\text{free}}(-\boldsymbol{\Delta}_\perp^2)$, the antisymmetric contribution to the energy density cancels the angular modulations that occurred in the symmetric EMT. Accordingly, for the asymmetric EMT, a synchronization-induced energy dipole moment arises from internal dynamics rather than being universally present in all fermions.

A benefit of the asymmetric EMT is that the energy and momentum *densities* are all trivial for a free elementary fermion, which appeals to intuition about the behavior of pointlike particles. The symmetric EMT, by contrast, suggests that pointlike fermions have non-trivial distributions of energy and momentum. To be sure, this picture seems more reasonable when recalling that fields are the fundamental objects of quantum field theories rather than particles; it is not farfetched to imagine that the fermion field can carry momentum around the center of an excitation in the field. For that matter, the flux densities in the asymmetric EMT of a free fermion are not zero, meaning that even the asymmetric EMT describes flows of energy and momentum—but flows that themselves contain zero momentum. In this regard, the symmetric EMT paints a more straightforward picture.

It would be instructive to obtain numerical estimates of the proton's EMT densities for the asymmetric EMT, and compare them with the results for the symmetric case. To this end, we assume the following multipole form for the spin form factor:

$$S(-\boldsymbol{\Delta}_\perp^2) = \frac{a_0/2}{(1 + \boldsymbol{\Delta}_\perp^2/m_{S1}^2)(1 + \boldsymbol{\Delta}_\perp^2/m_{S2}^2)} , \tag{98}$$

where for the mass poles we use the lightest isoscalar axial vector mesons identified by the Particle Data Group [78]:

$$m_{S1} = m(f_1(1285)) = 1281.9 \pm 0.5 \text{ MeV} \tag{99a}$$

$$m_{S2} = m(f_1(1420)) = 1426.3 \pm 0.9 \text{ MeV} , \tag{99b}$$

and for the zero-momentum value we use half the flavor-singlet axial vector charge of the proton, as determined by HERMES [86]:

$$a_0 = 0.330 \pm 0.011[\text{thy}] \pm 0.025[\text{exp}] \pm 0.028[\text{evo}] . \tag{100}$$

The 2D Fourier transform of the quantity appearing in all of Eqs. (94) (95), (96) and (97) evaluates in this model to:

$$m \int \frac{\mathrm{d}^2\boldsymbol{\Delta}_\perp}{(2\pi)^2} \frac{\mathrm{i}\boldsymbol{\Delta}_\perp}{2m} S(-\boldsymbol{\Delta}_\perp^2)\, \mathrm{e}^{-\mathrm{i}\boldsymbol{\Delta}_\perp \cdot \boldsymbol{b}_\perp} = \frac{a_0 \hat{b}_\perp}{8\pi} \frac{m_{S1}^2 m_{S2}^2}{m_{S2}^2 - m_{S1}^2} \Big(m_{S1} K_1(m_{S1} b_\perp) - m_{S2} K_1(m_{S2} b_\perp) \Big) \equiv \varSigma(\boldsymbol{b}_\perp) \hat{b}_\perp . \tag{101}$$

Another interesting quantity to consider is the density of quark spin around the z axis:

$$\mathcal{S}_z(\boldsymbol{b}_\perp, \hat{\boldsymbol{s}}) = \hat{e}_z \cdot \hat{\boldsymbol{s}} b_\perp \varSigma(\boldsymbol{b}_\perp) . \tag{102}$$

Numerical results for the quark spin in a longitudinally-polarized proton are given in Fig. 7. The error bands include only uncertainty in the parameters used, and not uncertainty arising from assuming a particular functional form. The error bands are dominated by uncertainty in the flavor singlet axial charge a_0, which does not contribute to the J_z density.

In Fig. 8, we present the energy density for a transversely-polarized proton using the asymmetric EMT. Qualitatively this looks similar to the analogous result for the symmetric EMT, shown in the right panel of Fig. 5. The lopsidedness of the density is slightly mitigated for the asymmetric EMT. In fact, rather than the universal synchronization-induced dipole moment of $-\hat{e}_z \times \hat{\boldsymbol{s}}/4$, the asymmetric EMT encodes a synchronization-induced energy dipole moment of:

$$\boldsymbol{d}_E = \left(-\frac{1}{4} + \frac{1}{2} S(0) \right) \hat{e}_z \times \hat{\boldsymbol{s}} = -(0.168 \pm 0.020)\, \hat{e}_z \times \hat{\boldsymbol{s}} , \tag{103}$$

meaning the energy dipole moment is only about 67% as big as for the symmetric EMT.

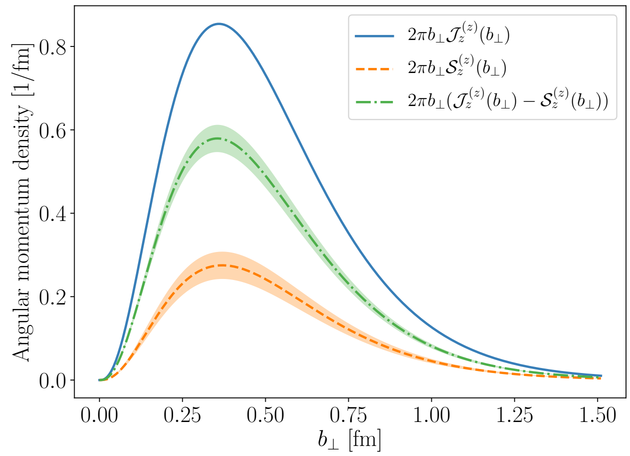

FIG. 7. One-dimensional reductions of the J_z density (defined in Eq. (68)) and the quark S_z density (defined in Eq. (102)) for a proton polarized along the z axis. In the absence of gluons, their difference (also plotted) would be an orbital angular momentum density, but in reality also contains the *total* gluon angular momentum distribution.

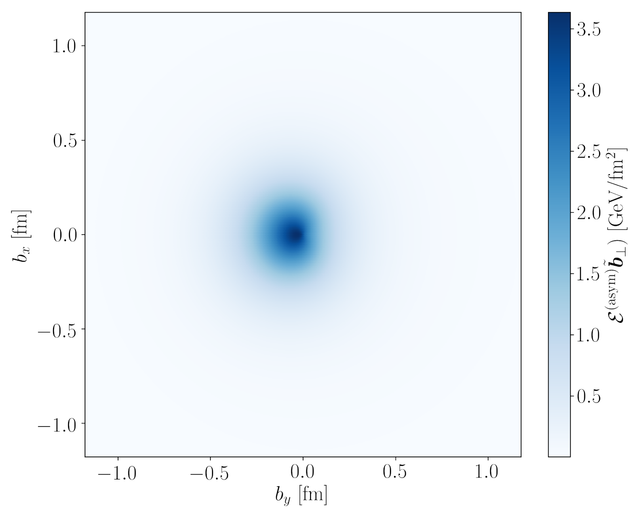

FIG. 8. The energy density as given in Eq. (97) for a proton polarized with spin-up along the x-axis. In this plot, the x-axis is oriented vertically and the y-axis horizontally so that the z axis points into the page, allowing plots to mimic what an observer would see at fixed light front time.

VI. CONCLUSIONS

In this work, we constructed and explored a formalism for obtaining exact, two-dimensional relativistic rest frame energy-momentum densities and currents for spin-zero and spin-half targets. We derived a general expression for these densities in terms of matrix elements of the EMT operator in Eq. (43), and subsequently obtained more explicit formulas for specific EMT components in terms of the gravitational form factors. Additionally, we provided numerical estimates for what these densities may look like for a proton, given the limited empirical data that exist.

The densities were obtained under a non-standard time synchronization convention via tilted light front coordinates, several effects of which can be seen in the results. In all targets (including spin-zero), there is a synchronization-induced energy flux in the z direction, related to the form factor $D(t)$, that results from asymmetry in the longitudinal velocity domain. (See Sec. IV D and Sec. IV E.) Since under light front synchronization the speed of light is infinite in the $-z$ direction and $1/2$ in the $+z$ direction, and the speeds of constituents within the target cannot exceed the speed of light, fluxes of constituents that would balance under the standard Einstein synchronization will no longer balance under light front synchronization. This clearly flags the emergence of a non-zero energy flux as an optical synchronization effect, and the very emergence of this effect provides a clear indication of motion within the hadron. Since the form factor $D(t)$ is widely believed to be related to internal pressures [8, 14–17], its appearance in the synchronization-induced flux suggests that—much like the hydrostatic pressure of fluids—a hadron's internal pressure comes from internal motion of its constituents. This calls into question interpretations of the internal pressures as providing information about long-range forces or confinement.

Additional synchronization effects were seen in spin-half targets, though these—much like the charge density modulations previously seen in light front densities [33, 87]—are related to rotational motion in transversely-polarized targets. The energy density of transversely-polarized targets has the peculiarity that its $\sin\phi$ modulations have the opposite sign from the modulations in any other density—in particular, energy bunches on the side of the target moving towards the observer rather than away. As discussed in Sec. V D, this is an artifact of the hadron's barycenter being the center-of-P_z rather than the center-of-energy. Curiously, the synchronization-induced energy dipole moment of a spin-half target is universally $-1/4$ if the symmetric Belinfante EMT is used to define the energy density—even for pointlike fermions. However, if the asymmetric EMT (defined by Leader and Lorcé [11]) is used instead, the energy dipole moment is non-universal and vanishes for pointlike fermions (see Sec. V F).

That the energy density should differ depending on whether the symmetric or asymmetric EMT is used may be the most peculiar and interesting of our results. It is not clear whether the energy density can be directly measured (as opposed to indirectly obtained by taking Fourier transforms of empirical gravitational form factors) so it is unclear that these cases can be empirically distinguished. Nonetheless, the energy density is one of the most preeminent desired quantities for describing hadron structure—being closely tied in with the mass decomposition and mass origin questions—and that the different EMT operators should entail different energy densities suggests that we ought to seriously consider which is more appropriate to use.

ACKNOWLEDGMENTS

We would like to thank Ian Cloët, Wim Cosyn, Yang Li, Cédric Lorcé, and Andreas Metz for thought-provoking conversations that helped contribute to this work. This work was supported by the U.S. Department of Energy Office of Science, Office of Nuclear Physics under Award Number DE-FG02-97ER-41014. AF was additionally supported by the U.S. Department of Energy contract No. DE-AC05-06OR23177, under which Jefferson Science Associates, LLC operates Jefferson Lab.

Appendix A: Basic identities in tilted light front coordinates

For convenience, we reproduce here several identities involving tilted light front coordinates from our previous work [33]. In this work, we do not use tildes to signify tilted coordinates, and expressions without explicit indication of the coordinate system should be assumed to be in tilted coordinates. By contrast, we explicitly signify instant form coordinates with a subscript or superscript IF.

Tilted light front coordinates are defined in terms of Minkowski (or instant form) coordinates as:

$$\tau = x^0 \equiv t_{\text{IF}} + z_{\text{IF}} \tag{A1a}$$
$$x = x^1 \equiv x_{\text{IF}} \tag{A1b}$$
$$y = x^2 \equiv y_{\text{IF}} \tag{A1c}$$
$$z = x^3 \equiv z_{\text{IF}} \,. \tag{A1d}$$

In this way, tilted coordinates operationally correspond to a change in the way that spatially distant clocks are synchronized [33, 41, 44, 45]. The metric tensor and its inverse are:

$$g_{\mu\nu} = \frac{\partial x^\alpha_{\text{IF}}}{\partial x^\mu}\frac{\partial x^\beta_{\text{IF}}}{\partial x^\nu} g_{\alpha\beta} = \begin{bmatrix} 1 & 0 & 0 & -1 \\ 0 & -1 & 0 & 0 \\ 0 & 0 & -1 & 0 \\ -1 & 0 & 0 & 0 \end{bmatrix} \tag{A2a}$$

$$g^{\mu\nu} = \frac{\partial x^\mu}{\partial x^\alpha_{\text{IF}}}\frac{\partial x^\nu}{\partial x^\beta_{\text{IF}}} g^{\alpha\beta} = \begin{bmatrix} 0 & 0 & 0 & -1 \\ 0 & -1 & 0 & 0 \\ 0 & 0 & -1 & 0 \\ -1 & 0 & 0 & -1 \end{bmatrix} \tag{A2b}$$

Covariant (lower-index) and contravariant (upper-index) four-vector components are related by:

$$A_\mu = g_{\mu\nu} A^\nu \qquad\qquad A^\mu = g^{\mu\nu} A_\nu \,, \tag{A3a}$$

which in terms of individual components gives:

$$A_0 = A^0 - A^3 \qquad A^0 = -A_3 \tag{A3b}$$
$$A_1 = -A^1 \qquad A^1 = -A_1 \tag{A3c}$$
$$A_2 = -A^2 \qquad A^2 = -A_2 \tag{A3d}$$
$$A_3 = -A^0 \qquad A^3 = -A_0 - A_3\,. \tag{A3e}$$

The energy and momentum are defined to be time and space translation generators:

$$i[E, \hat{O}(x)] = \partial_0 \hat{O}(x) \tag{A4a}$$
$$-i[\boldsymbol{p}, \hat{O}(x)] = \boldsymbol{\nabla} \hat{O}(x)\,, \tag{A4b}$$

meaning they are related to covariant (lower-index) components of the four-momentum p_μ:

$$p_\mu \equiv (E; -p_x, -p_y, -p_z)\,. \tag{A5}$$

The tilted coordinate energy and momentum have the following relationships to instant form energy and momentum:

$$E = E^{\mathrm{IF}} \tag{A6a}$$
$$p_x = p_x^{\mathrm{IF}} \tag{A6b}$$
$$p_y = p_y^{\mathrm{IF}} \tag{A6c}$$
$$p_z = E^{\mathrm{IF}} + p_z^{\mathrm{IF}}\,. \tag{A6d}$$

The energy of a particle with mass m is given by:

$$E = \frac{m^2 + \boldsymbol{p}^2}{2p_z}\,, \tag{A7}$$

The momentum and velocity are related in the following way:

$$v_x = \frac{p_x}{p_z} \tag{A8a}$$
$$v_y = \frac{p_y}{p_z} \tag{A8b}$$
$$v_z = 1 - \frac{E}{p_z}\,. \tag{A8c}$$

Notably, at rest, one has $\boldsymbol{p}_{\text{rest}} = (0, 0, m)$. This occurs because p_z is defined to be the generator of translations rather than to be proportional to velocity.

As usual, boosts transform contravariant four-vectors according to the formula:

$$A'^\mu = \Lambda^\mu{}_\nu A^\nu\,. \tag{A9}$$

An active transverse boost can be written in matrix form as:

$$(\Lambda_\perp)^\mu{}_\nu = \begin{bmatrix} 1 & 0 & 0 & 0 \\ \beta_x & 1 & 0 & 0 \\ \beta_y & 0 & 1 & 0 \\ -\boldsymbol{\beta}_\perp^2/2 & -\beta_x & -\beta_y & 1 \end{bmatrix}, \tag{A10}$$

where $\boldsymbol{\beta}_\perp = (\beta_x, \beta_y)$ is the velocity of the boost. An active longitudinal boost can be written:

$$(\Lambda_\parallel)^\mu{}_\nu = \begin{bmatrix} \mathrm{e}^\eta & 0 & 0 & 0 \\ 0 & 1 & 0 & 0 \\ 0 & 0 & 1 & 0 \\ \sinh\eta & 0 & 0 & \mathrm{e}^{-\eta} \end{bmatrix}. \tag{A11}$$

Here, η is the rapidity of the longitudinal boost, and is related to the velocity v_z of the boost by:

$$\beta_z^\parallel = \mathrm{e}^{-\eta}\sinh(\eta) = \frac{1}{2}\left(1 - \mathrm{e}^{-2\eta}\right). \tag{A12}$$

As discussed in the main text, we consider states with arbitrary momentum $\boldsymbol{p}$ to be reached from the rest state through a longitudinal boost followed by a transverse boost. This combined boost can be written:

$$(\Lambda)^{\mu}{}_{\nu} = (\Lambda_{\perp}\Lambda_{\parallel})^{\mu}{}_{\nu} = \begin{bmatrix} \mathrm{e}^{\eta} & 0 & 0 & 0 \\ \mathrm{e}^{\eta}\beta_x & 1 & 0 & 0 \\ \mathrm{e}^{\eta}\beta_y & 0 & 1 & 0 \\ \mathrm{e}^{\eta}\beta_z & -\beta_x & -\beta_y & \mathrm{e}^{-\eta} \end{bmatrix}. \tag{A13}$$

Here,

$$\beta_z = \mathrm{e}^{-\eta}\sinh(\eta) - \frac{\boldsymbol{\beta}_{\perp}^2}{2} = \beta_z^{\parallel} - \frac{\boldsymbol{\beta}_{\perp}^2}{2}, \tag{A14}$$

as light front transverse boosts impart longitudinal velocity to the system, so the total longitudinal velocity of the combined boost differs from that of the longitudinal boost alone. Notably, the transverse boosts are defined to leave p_z invariant, but the relationship between p_z and v_z (see Eq. (A8)) means that v_z must change. From Eqs. (A7) and (A8), the boost that takes a system from rest to an arbitrary momentum $\boldsymbol{p}$ can be written in terms of its energy and momentum as:

$$\Lambda^{\mu}{}_{\nu} = \begin{bmatrix} p_z/m & 0 & 0 & 0 \\ p_x/m & 1 & 0 & 0 \\ p_y/m & 0 & 1 & 0 \\ (p_z - E)/m & -p_x/p_z & -p_y/p_z & m/p_z \end{bmatrix}. \tag{A15}$$

Appendix B: Explicit matrix forms of four-vectors and tensors

To efficiently calculate intrinsic densities according to Eqs. (41) and (43), it is helpful to have explicit matrix forms for the matrix $\bar{\Lambda}^{\mu}{}_{\nu}$ and its inverse, as well as four-vectors that appear in the relevant matrix elements. This Appendix provides these explicit matrix forms.

1. Matrix form of Lorentz boost and its inverse

As discussed in Sec. III of the main text, $\bar{\Lambda}^{\mu}{}_{\nu}$ is not actually a Lorentz transform, but an average of Lorentz transforms from rest to four-momenta p_μ and p'_μ. These four-momenta have the same $P_z = p_z = p'_z$ by virtue of the z coordinate being integrated out, and since the boosts (as given in Eq. (A15)) are linear in the other components of the four-momentum, one can obtain $\bar{\Lambda}^{\mu}{}_{\nu}$ by substituting $p_\mu \mapsto P_\mu \equiv \frac{1}{2}\big(p + p'\big)$ into Eq. (A15). The resulting matrix and its inverse are:

$$\bar{\Lambda}^{\mu}{}_{\nu} = \begin{bmatrix} P_z/m & 0 & 0 & 0 \\ P_x/m & 1 & 0 & 0 \\ P_y/m & 0 & 1 & 0 \\ (P_z - P_0)/m & -P_x/P_z & -P_y/P_z & m/P_z \end{bmatrix} \tag{B1a}$$

$$(\bar{\Lambda}^{-1})^{\mu}{}_{\nu} = \begin{bmatrix} m/P_z & 0 & 0 & 0 \\ -P_x/P_z & 1 & 0 & 0 \\ -P_y/P_z & 0 & 1 & 0 \\ P_0/m - \boldsymbol{P}^2/(mP_z) & P_x/m & P_y/m & P_z/m \end{bmatrix} \tag{B1b}$$

where

$$P_0 = \frac{1}{2}\Big(E_{\boldsymbol{p}} + E_{\boldsymbol{p}'}\Big) = \frac{m^2 + \boldsymbol{P}^2}{2P_z} + \frac{\boldsymbol{\Delta}_{\perp}^2}{8P_z} \tag{B2}$$

given $\Delta = p' - p$ and $\Delta_z = 0$. This averaged boost alters covariant (lower-index) four-vectors through $A'_\mu = \bar{\Lambda}_{\mu}{}^{\nu}A_\nu$, where $\bar{\Lambda}_{\mu}{}^{\nu} = g_{\mu\alpha}g^{\nu\beta}\bar{\Lambda}^{\alpha}{}_{\beta}$. ($g_{\mu\nu}$ and $g^{\mu\nu}$ are given in Eq. (A2).) However, it is easier in practice to transform the contravariant form of a four-vector and then use the metric to lower the index, i.e. to raise the index via $A^\mu = g^{\mu\nu}A_\nu$, evaluate $A'^\mu = \bar{\Lambda}^{\mu}{}_{\nu}A^\nu$, and then lower the index again via $A'_\mu = g_{\mu\nu}A'^\nu$. We will thus only give explicit evaluations for transformations of contravariant four-vectors.

2. Matrix forms of contravariant four-vectors

The time and energy projection vectors $n_\mu = (1; 0, 0, 0)$ and $\bar{n}^\mu = (1; 0, 0, 0)$, are, in contravariant form:

$$n^\mu = \begin{bmatrix} 0 \\ 0 \\ 0 \\ -1 \end{bmatrix} \qquad \bar{n}^\mu = \begin{bmatrix} 1 \\ 0 \\ 0 \\ 0 \end{bmatrix} . \tag{B3}$$

Only the former appears in the QFT matrix elements, but the latter appears in the inverse-boosted expressions.

We next consider the average four-momentum P^μ and the momentum transfer Δ^μ. In the context of Eqs. (41) and (43), $\Delta_z = 0$ and accordingly

$$\Delta_0 = \frac{\boldsymbol{\Delta}_\perp \cdot \boldsymbol{P}_\perp}{P_z} , \tag{B4}$$

and thus:

$$P^\mu = \begin{bmatrix} P_z \\ P_x \\ P_y \\ P_z - P_0 \end{bmatrix} \qquad \Delta^\mu = \begin{bmatrix} 0 \\ \Delta_x \\ \Delta_y \\ -\boldsymbol{\Delta}_\perp \cdot \boldsymbol{P}_\perp / P_z \end{bmatrix} . \tag{B5}$$

There are several four-vectors that appear in matrix elements of spin-half targets. One of these is:

$$-\frac{\mathrm{i}\epsilon^{\mu\nu\rho\sigma} n_\nu P \rho \Delta_\sigma}{P \cdot n} (\sigma_3)_{\lambda'\lambda} = \begin{bmatrix} 0 \\ \mathrm{i}\Delta_y \\ -\mathrm{i}\Delta_x \\ \mathrm{i}(\boldsymbol{P} \times \boldsymbol{\Delta}_\perp) \cdot \hat{e}_z / P_z \end{bmatrix} (\sigma_3)_{\lambda'\lambda} , \tag{B6a}$$

and the other is:

$$\frac{m n^\mu}{(P \cdot n)} \mathrm{i}\epsilon^{\alpha\beta\gamma\delta} n_\alpha \bar{n}_\beta \Delta_\gamma (\sigma_\delta)_{\lambda'\lambda} = \frac{m}{P_z} \mathrm{i}(\boldsymbol{\sigma}_{\lambda'\lambda} \times \boldsymbol{\Delta}_\perp) \cdot \hat{e}_z \begin{bmatrix} 0 \\ 0 \\ 0 \\ 1 \end{bmatrix} , \tag{B6b}$$

where the helpful relation:

$$\mathrm{i}\epsilon^{\alpha\beta\gamma\delta} n_\alpha \bar{n}_\beta \Delta_\gamma (\sigma_\delta)_{\lambda'\lambda} = -\mathrm{i}(\boldsymbol{\sigma}_{\lambda'\lambda} \times \boldsymbol{\Delta}_\perp) \cdot \hat{e}_z \tag{B7}$$

from Appendix A of Ref. [33] was used.

3. Matrix forms of transformed four-vectors

We now present the results of $\bar{\Lambda}^{-1}$ acting on each of the four-vectors above (except for $\bar{n}^\mu$), since these appear in Eqs. (41) and (43).

Using Eqs. (B1) and (B3), we find:

$$(\bar{\Lambda}^{-1} n)^\mu = \begin{bmatrix} 0 \\ 0 \\ 0 \\ -P_z/m \end{bmatrix} . \tag{B8}$$

Next, using Eqs. (B1) and (B5), we find:

$$(\bar{\Lambda}^{-1} P)^\mu = \begin{bmatrix} m \\ 0 \\ 0 \\ 0 \end{bmatrix} = m\bar{n}^\mu \qquad (\bar{\Lambda}^{-1} \Delta)^\mu = \begin{bmatrix} 0 \\ \Delta_x \\ \Delta_y \\ 0 \end{bmatrix} \equiv \Delta_\perp^\mu . \tag{B9}$$

Lastly, using using Eqs. (B1) and (B6), we find:

$$-(\bar{\Lambda}^{-1})^{\mu}{}_{\zeta}\,\frac{\mathrm{i}\epsilon^{\zeta\nu\rho\sigma}n_\nu P\rho\Delta_\sigma}{P\cdot n}(\sigma_3)_{\lambda'\lambda} = \begin{bmatrix} 0 \\ \mathrm{i}\Delta_y \\ -i\Delta_x \\ 0 \end{bmatrix}(\sigma_3)_{\lambda'\lambda} = \mathrm{i}\big((\sigma_3)_{\lambda'\lambda}\hat{e}_z \times \boldsymbol{\Delta}_\perp\big)^{\mu} \tag{B10a}$$

$$(\bar{\Lambda}^{-1})^{\mu}{}_{\zeta}\,\frac{mn^{\zeta}}{(P\cdot n)}\,\mathrm{i}\epsilon^{\alpha\beta\gamma\delta}n_\alpha\bar{n}_\beta\Delta_\gamma(\sigma_\delta)_{\lambda'\lambda} = \mathrm{i}(\boldsymbol{\sigma}_{\lambda'\lambda}\times\boldsymbol{\Delta}_\perp)\cdot\hat{e}_z \begin{bmatrix} 0 \\ 0 \\ 0 \\ 1 \end{bmatrix}. \tag{B10b}$$

Adding both of these conveniently gives:

$$(\bar{\Lambda}^{-1})^{\mu}{}_{\zeta}\left\{-\frac{\mathrm{i}\epsilon^{\zeta\nu\rho\sigma}n_\nu P\rho\Delta_\sigma}{P\cdot n}(\sigma_3)_{\lambda'\lambda} + \frac{mn^{\zeta}}{(P\cdot n)}\,\mathrm{i}\epsilon^{\alpha\beta\gamma\delta}n_\alpha\bar{n}_\beta\Delta_\gamma(\sigma_\delta)_{\lambda'\lambda}\right\} = \mathrm{i}(\boldsymbol{\sigma}_{\lambda'\lambda}\times\boldsymbol{\Delta}_\perp)^{\mu}\,. \tag{B10c}$$

4. Transformation of the metric

In matrix elements of the energy-momentum tensor, the metric tensor $g^{\mu\mu}$ explicitly appears along with the form factor $D(\Delta^2)$. If $\bar{\Lambda}$ were a proper Lorentz transform, one would find $\bar{\Lambda}^{\mu}{}_{\alpha}\bar{\Lambda}^{\nu}{}_{\beta}g^{\alpha\beta} = g^{\mu\nu}$, but this is not the case.

This can be shown through explicitly matrix multiplication. Since $g^{\mu\nu}$ are components of the inverse metric (given in Eq. (A2)), the relevant quantities are $\bar{\Lambda}g^{-1}\bar{\Lambda}^{\mathsf{T}}$ and $\bar{\Lambda}^{-1}g^{-1}(\bar{\Lambda}^{-1})^{\mathsf{T}}$. These evaluate to:

$$\left(\bar{\Lambda}g^{-1}\bar{\Lambda}^{\mathsf{T}}\right)^{\mu\nu} = g^{\mu\nu} + \frac{\boldsymbol{\Delta}_\perp^2}{4mP_z}\begin{bmatrix} 0&0&0&0\\0&0&0&0\\0&0&0&0\\0&0&0&1\end{bmatrix} = g^{\mu\nu} + \frac{\boldsymbol{\Delta}_\perp^2}{4mP_z}n^{\mu}n^{\nu} \tag{B11a}$$

$$\left(\bar{\Lambda}^{-1}g^{-1}(\bar{\Lambda}^{-1})^{\mathsf{T}}\right)^{\mu\nu} = g^{\mu\nu} - \frac{\boldsymbol{\Delta}_\perp^2}{4mP_z}\begin{bmatrix} 0&0&0&0\\0&0&0&0\\0&0&0&0\\0&0&0&1\end{bmatrix} = g^{\mu\nu} - \frac{\boldsymbol{\Delta}_\perp^2}{4mP_z}n^{\mu}n^{\nu}\,. \tag{B11b}$$

Thus, since Lorentz transforms are defined to leave the metric invariant, $\bar{\Lambda}^{\mu}{}_{\nu}$ is not a Lorentz transform. However, as explained in the text, it only plays the role of encoding momentum dependence of matrix elements; it is not used as a Lorentz boost.

---

[1] I. Yu. Kobzarev and L. B. Okun, "Gravitational interaction of fermions," Zh. Eksp. Teor. Fiz. **43**, 1904–1909 (1962).
[2] Xiang-Dong Ji, "A QCD analysis of the mass structure of the nucleon," Phys. Rev. Lett. **74**, 1071–1074 (1995), arXiv:hep-ph/9410274.
[3] Xiang-Dong Ji, "Breakup of hadron masses and energy - momentum tensor of QCD," Phys. Rev. D **52**, 271–281 (1995), arXiv:hep-ph/9502213.
[4] Cédric Lorcé, "On the hadron mass decomposition," Eur. Phys. J. C **78**, 120 (2018), arXiv:1706.05853 [hep-ph].
[5] Yoshitaka Hatta, Abha Rajan, and Kazuhiro Tanaka, "Quark and gluon contributions to the QCD trace anomaly," JHEP **12**, 008 (2018), arXiv:1810.05116 [hep-ph].
[6] Andreas Metz, Barbara Pasquini, and Simone Rodini, "Revisiting the proton mass decomposition," Phys. Rev. D **102**, 114042 (2021), arXiv:2006.11171 [hep-ph].
[7] Xiangdong Ji, "Proton mass decomposition: naturalness and interpretations," Front. Phys. (Beijing) **16**, 64601 (2021), arXiv:2102.07830 [hep-ph].
[8] Cédric Lorcé, Andreas Metz, Barbara Pasquini, and Simone Rodini, "Energy-momentum tensor in QCD: nucleon mass decomposition and mechanical equilibrium," JHEP **11**, 121 (2021), arXiv:2109.11785 [hep-ph].
[9] J. Ashman *et al.* (European Muon), "A Measurement of the Spin Asymmetry and Determination of the Structure Function g(1) in Deep Inelastic Muon-Proton Scattering," Phys. Lett. B **206**, 364 (1988).
[10] Xiang-Dong Ji, "Gauge-Invariant Decomposition of Nucleon Spin," Phys. Rev. Lett. **78**, 610–613 (1997), arXiv:hep-ph/9603249.
[11] E. Leader and C. Lorcé, "The angular momentum controversy: What's it all about and does it matter?" Phys. Rept. **541**, 163–248 (2014), arXiv:1309.4235 [hep-ph].
[12] Masashi Wakamatsu, "Is gauge-invariant complete decomposition of the nucleon spin possible?" Int. J. Mod. Phys. A **29**, 1430012 (2014), arXiv:1402.4193 [hep-ph].
[13] Xiangdong Ji, Feng Yuan, and Yong Zhao, "What we know and what we don't know about the proton spin after 30 years," Nature Rev. Phys. **3**, 27–38 (2021), arXiv:2009.01291 [hep-ph].

[14] M. V. Polyakov, "Generalized parton distributions and strong forces inside nucleons and nuclei," Phys. Lett. B **555**, 57–62 (2003), arXiv:hep-ph/0210165.
[15] Maxim V. Polyakov and Peter Schweitzer, "Forces inside hadrons: pressure, surface tension, mechanical radius, and all that," Int. J. Mod. Phys. A **33**, 1830025 (2018), arXiv:1805.06596 [hep-ph].
[16] Cédric Lorcé, Hervé Moutarde, and Arkadiusz P. Trawiński, "Revisiting the mechanical properties of the nucleon," Eur. Phys. J. C **79**, 89 (2019), arXiv:1810.09837 [hep-ph].
[17] Adam Freese and Gerald A. Miller, "Forces within hadrons on the light front," Phys. Rev. D **103**, 094023 (2021), arXiv:2102.01683 [hep-ph].
[18] Xiangdong Ji and Yizhuang Liu, "Momentum-Current Gravitational Multipoles of Hadrons," Phys. Rev. D **106**, 034028 (2022), arXiv:2110.14781 [hep-ph].
[19] Daniel Boer *et al.*, "Gluons and the quark sea at high energies: Distributions, polarization, tomography," (2011), arXiv:1108.1713 [nucl-th].
[20] A. Accardi *et al.*, "Electron Ion Collider: The Next QCD Frontier: Understanding the glue that binds us all," Eur. Phys. J. A **52**, 268 (2016), arXiv:1212.1701 [nucl-ex].
[21] R. Abdul Khalek *et al.*, "Science Requirements and Detector Concepts for the Electron-Ion Collider: EIC Yellow Report," (2021), arXiv:2103.05419 [physics.ins-det].
[22] Xiang-Dong Ji, "Deeply virtual Compton scattering," Phys. Rev. D **55**, 7114–7125 (1997), arXiv:hep-ph/9609381.
[23] A. V. Radyushkin, "Nonforward parton distributions," Phys. Rev. D **56**, 5524–5557 (1997), arXiv:hep-ph/9704207.
[24] A. V. Belitsky and A. V. Radyushkin, "Unraveling hadron structure with generalized parton distributions," Phys. Rept. **418**, 1–387 (2005), arXiv:hep-ph/0504030.
[25] Gordon N. Fleming, "Charge Distributions from Relativistic Form-Factors," in *Physical reality and mathematical description: Festschrift Jauch (Josef Maria) on his 60th birthday*, edited by Charles P. Enz and Jagdish Mehra (1974) pp. 357–374.
[26] Matthias Burkardt, "Impact parameter dependent parton distributions and off forward parton distributions for zeta —> 0," Phys. Rev. D **62**, 071503 (2000), [Erratum: Phys.Rev.D 66, 119903 (2002)], arXiv:hep-ph/0005108.
[27] Gerald A. Miller, "Defining the proton radius: A unified treatment," Phys. Rev. C **99**, 035202 (2019), arXiv:1812.02714 [nucl-th].
[28] E. Epelbaum, J. Gegelia, N. Lange, U. G. Meißner, and M. V. Polyakov, "Definition of Local Spatial Densities in Hadrons," Phys. Rev. Lett. **129**, 012001 (2022), arXiv:2201.02565 [hep-ph].
[29] Yang Li, Wen-bo Dong, Yi-liang Yin, Qun Wang, and James P. Vary, "Minkowski's lost legacy and hadron electromagnetism," Phys. Lett. B **838**, 137676 (2023), arXiv:2206.12903 [hep-ph].
[30] Yi Chen and Cédric Lorcé, "Pion and nucleon relativistic electromagnetic four-current distributions," Phys. Rev. D **106**, 116024 (2022), arXiv:2210.02908 [hep-ph].
[31] Adam Freese and Gerald A. Miller, "On the true meaning of spatial densities of hadrons," (2022), arXiv:2210.03807 [hep-ph].
[32] J. Yu. Panteleeva, E. Epelbaum, J. Gegelia, and U. G. Meißner, "Definition of gravitational local spatial densities for spin-0 and spin-1/2 systems," (2022), arXiv:2211.09596 [hep-ph].
[33] Adam Freese and Gerald A. Miller, "Light front synchronization and rest frame densities of the proton: Electromagnetic densities," Phys. Rev. D **107**, 074036 (2023), arXiv:2302.09171 [hep-ph].
[34] Yi Chen and Cédric Lorcé, "Nucleon relativistic polarization and magnetization distributions," Phys. Rev. D **107**, 096003 (2023), arXiv:2302.04672 [hep-ph].
[35] J. Yu. Panteleeva, E. Epelbaum, J. Gegelia, and U. G. Meißner, "Electromagnetic and gravitational local spatial densities for spin-1 systems," (2023), arXiv:2305.01491 [hep-ph].
[36] Matthias Burkardt, "Impact parameter space interpretation for generalized parton distributions," Int. J. Mod. Phys. A **18**, 173–208 (2003), arXiv:hep-ph/0207047.
[37] Gerald A. Miller, "Transverse Charge Densities," Ann. Rev. Nucl. Part. Sci. **60**, 1–25 (2010), arXiv:1002.0355 [nucl-th].
[38] Cédric Lorcé, "Charge Distributions of Moving Nucleons," Phys. Rev. Lett. **125**, 232002 (2020), arXiv:2007.05318 [hep-ph].
[39] P. G. Blunden, M. Burkardt, and G. A. Miller, "Light front nuclear physics: Toy models, static sources and tilted light front coordinates," Phys. Rev. C **61**, 025206 (2000), arXiv:nucl-th/9908067.
[40] Albert Einstein, "On the electrodynamics of moving bodies," Annalen Phys. **17**, 891–921 (1905).
[41] H. Reichenbach, *The Philosophy of Space and Time*, Dover Books on Physics (Dover Publications, 2012).
[42] A. Grünbaum, *Philosophical Problems of Space and Time: Second, enlarged edition*, Boston Studies in the Philosophy and History of Science (Springer Netherlands, 2012).
[43] Yuan Zhong Zhang, "Test theories of special relativity," General Relativity and Gravitation **27**, 475–493 (1995).
[44] Ronald Anderson, Geoffrey E. Stedman, and I. Vetharaniam, "Conventionality of synchronisation, gauge dependence and test theories of relativity," Phys. Rept. **295**, 93–180 (1998).
[45] Derek Muller and Petr Lebedev, "Why No One Has Measured The Speed Of Light," (2020).
[46] J. Yu. Panteleeva, E. Epelbaum, J. Gegelia, and U. G. Meißner, "On the definition of electromagnetic local spatial densities for composite spin-$1/2$ systems," (2022), arXiv:2205.15061 [hep-ph].
[47] Adam Freese and Gerald A. Miller, "Unified formalism for electromagnetic and gravitational probes: Densities," Phys. Rev. D **105**, 014003 (2022), arXiv:2108.03301 [hep-ph].
[48] Taichiro Kugo and Izumi Ojima, "Local Covariant Operator Formalism of Nonabelian Gauge Theories and Quark Confinement Problem," Prog. Theor. Phys. Suppl. **66**, 1–130 (1979).
[49] F. J. Belinfante, "On the spin angular momentum of mesons," Physica **6**, 887–898 (1939).
[50] Adam Freese, "Noether's theorems and the energy-momentum tensor in quantum gauge theories," Phys. Rev. D **106**, 125012 (2022), arXiv:2112.00047 [hep-th].
[51] Alexander L Fetter and John Dirk Walecka, *Theoretical mechanics of particles and continua*, International series in pure and applied

physics (McGraw-Hill, New York, NY, 1980).
[52] C.K. Batchelor and G.K. Batchelor, *An Introduction to Fluid Dynamics*, Cambridge Mathematical Library (Cambridge University Press, 2000).
[53] F. Irgens, *Continuum Mechanics* (Springer Berlin Heidelberg, 2008).
[54] John L. Friedman and Nikolaos Stergioulas, *Rotating Relativistic Stars*, Cambridge Monographs on Mathematical Physics (Cambridge University Press, 2013).
[55] W. Flügge, *Tensor Analysis and Continuum Mechanics* (Springer Berlin Heidelberg, 2013).
[56] I.S. Liu, *Continuum Mechanics*, Advanced Texts in Physics (Springer Berlin Heidelberg, 2013).
[57] A.F. Bower, *Applied Mechanics of Solids* (CRC Press, 2009).
[58] J. L. Ericksen, "Conservation Laws for Liquid Crystals," Transactions of The Society of Rheology **5**, 23–34 (1961), https://pubs.aip.org/sor/jor/article-pdf/5/1/23/12261492/1_548883.pdf.
[59] Dieter Forster, Tom C. Lubensky, Paul C. Martin, Jack Swift, and P. S. Pershan, "Hydrodynamics of liquid crystals," Phys. Rev. Lett. **26**, 1016–1019 (1971).
[60] Helmut R. Brand and Harald Pleiner, "Two-fluid model for the breakdown of flow alignment in nematic liquid crystals," Phys. Rev. E **103**, 012705 (2021).
[61] John L. Friedman, James R. Ipser, and Subrahmanyan Chandrasekhar, "Rapidly rotating relativistic stars," Philosophical Transactions of the Royal Society of London. Series A: Physical and Engineering Sciences **340**, 391–422 (1992), https://royalsocietypublishing.org/doi/pdf/10.1098/rsta.1992.0074.
[62] P. C. Martin, O. Parodi, and P. S. Pershan, "Unified hydrodynamic theory for crystals, liquid crystals, and normal fluids," Phys. Rev. A **6**, 2401–2420 (1972).
[63] Hilbrand Johannes Groenewold, "On the principles of elementary quantum mechanics," in *On the Principles of Elementary Quantum Mechanics* (Springer Netherlands, Dordrecht, 1946) pp. 1–56.
[64] Ivan Todorov, ""quantization is a mystery"," (2012), arXiv:1206.3116 [math-ph].
[65] C. Itzykson and J.B. Zuber, *Quantum Field Theory*, International Series In Pure and Applied Physics (McGraw-Hill, New York, 1980).
[66] Cédric Lorcé and Peter Lowdon, "Analytic constraints on the energy-momentum tensor in conformal field theories," Phys. Rev. D **102**, 125013 (2020), arXiv:2004.13057 [hep-th].
[67] I. A. Perevalova, M. V. Polyakov, and P. Schweitzer, "On LHCb pentaquarks as a baryon-ψ(2S) bound state: prediction of isospin-$\frac{3}{2}$ pentaquarks with hidden charm," Phys. Rev. D **94**, 054024 (2016), arXiv:1607.07008 [hep-ph].
[68] Adam Freese and Gerald A. Miller, "Genuine empirical pressure within the proton," Phys. Rev. D **104**, 014024 (2021), arXiv:2104.03213 [hep-ph].
[69] Cédric Lorcé, "The relativistic center of mass in field theory with spin," Eur. Phys. J. C **78**, 785 (2018), arXiv:1805.05284 [hep-ph].
[70] O. V. Teryaev, "Spin structure of nucleon and equivalence principle," (1999), arXiv:hep-ph/9904376.
[71] Jonathan Hudson and Peter Schweitzer, "Dynamic origins of fermionic D-terms," Phys. Rev. D **97**, 056003 (2018), arXiv:1712.05317 [hep-ph].
[72] V. D. Burkert, L. Elouadrhiri, and F. X. Girod, "The pressure distribution inside the proton," Nature **557**, 396–399 (2018).
[73] V. D. Burkert, L. Elouadrhiri, and F. X. Girod, "Determination of shear forces inside the proton," (2021), arXiv:2104.02031 [nucl-ex].
[74] Krešimir Kumerički, "Measurability of pressure inside the proton," Nature **570**, E1–E2 (2019).
[75] B. Duran *et al.*, "Determining the gluonic gravitational form factors of the proton," Nature **615**, 813–816 (2023), arXiv:2207.05212 [nucl-ex].
[76] Yuxun Guo, Xiangdong Ji, Yizhuang Liu, and Jinghong Yang, "Updated analysis of near-threshold heavy quarkonium production for probe of proton's gluonic gravitational form factors," (2023), arXiv:2305.06992 [hep-ph].
[77] Pere Masjuan, Enrique Ruiz Arriola, and Wojciech Broniowski, "Meson dominance of hadron form factors and large-N_c phenomenology," Phys. Rev. D **87**, 014005 (2013), arXiv:1210.0760 [hep-ph].
[78] R. L. Workman *et al.* (Particle Data Group), "Review of Particle Physics," PTEP **2022**, 083C01 (2022).
[79] P. E. Shanahan and W. Detmold, "Gluon gravitational form factors of the nucleon and the pion from lattice QCD," Phys. Rev. D **99**, 014511 (2019), arXiv:1810.04626 [hep-lat].
[80] Dimitra A. Pefkou, Daniel C. Hackett, and Phiala E. Shanahan, "Gluon gravitational structure of hadrons of different spin," Phys. Rev. D **105**, 054509 (2022), arXiv:2107.10368 [hep-lat].
[81] DLMF, "*NIST Digital Library of Mathematical Functions*," http://dlmf.nist.gov/, Release 1.1.0 of 2020-12-15, f. W. J. Olver, A. B. Olde Daalhuis, D. W. Lozier, B. I. Schneider, R. F. Boisvert, C. W. Clark, B. R. Miller, B. V. Saunders, H. S. Cohl, and M. A. McClain, eds.
[82] Gerald A. Miller, "Singular Charge Density at the Center of the Pion?" Phys. Rev. C **79**, 055204 (2009), arXiv:0901.1117 [nucl-th].
[83] Julia Yu. Panteleeva and Maxim V. Polyakov, "Forces inside the nucleon on the light front from 3D Breit frame force distributions: Abel tomography case," Phys. Rev. D **104**, 014008 (2021), arXiv:2102.10902 [hep-ph].
[84] Brandon Kriesten, Simonetta Liuti, Liliet Calero-Diaz, Dustin Keller, Andrew Meyer, Gary R. Goldstein, and J. Osvaldo Gonzalez-Hernandez, "Extraction of Generalized Parton Distribution Observables from Deeply Virtual Electron Proton Scattering Experiments," Phys. Rev. D **101**, 054021 (2020), arXiv:1903.05742 [hep-ph].
[85] Jian-Wei Qiu and Zhite Yu, "Single diffractive hard exclusive processes for the study of generalized parton distributions," Phys. Rev. D **107**, 014007 (2023), arXiv:2210.07995 [hep-ph].
[86] A. Airapetian *et al.* (HERMES), "Precise determination of the spin structure function g(1) of the proton, deuteron and neutron," Phys. Rev. D **75**, 012007 (2007), arXiv:hep-ex/0609039.
[87] Carl E. Carlson and Marc Vanderhaeghen, "Empirical transverse charge densities in the nucleon and the nucleon-to-Delta transition," Phys. Rev. Lett. **100**, 032004 (2008), arXiv:0710.0835 [hep-ph].